NASA CONTRACTOR
REPORT

NASA CR-144293

OBSERVATION OF ACOUSTIC-GRAVITY WAVES IN THE UPPER ATMOSPHERE DURING SEVERE STORM ACTIVITY

By R. J. Hung

School of Graduate Studies and Research
The University of Alabama in Huntsville
Huntsville, Alabama 35807

July 1975

Prepared for

NASA-GEORGE C. MARSHALL SPACE FLIGHT CENTER
Marshall Space Flight Center, Alabama 35812

TECHNICAL REPORT STANDARD TITLE PAGE

1 REPORT NO.	2. GOVERNMENT ACCESSION NO.	3. RECIPIENT'S CATALOG NO.
NASA CR-144293		

4 TITLE AND SUBTITLE	5. REPORT DATE
Observation of Acoustic-Gravity Waves in the Upper Atmosphere During Severe Storm Activity	July 1975
	6. PERFORMING ORGANIZATION CODE
7. AUTHOR(S)	8. PERFORMING ORGANIZATION REPORT #
R. J. Hung	
9. PERFORMING ORGANIZATION NAME AND ADDRESS	10. WORK UNIT NO.
School of Graduate Studies and Research The University of Alabama in Huntsville Huntsville, Alabama 35807	11. CONTRACT OR GRANT NO. NAS8-30616
12 SPONSORING AGENCY NAME AND ADDRESS	13. TYPE OF REPORT & PERIOD COVERED
National Aeronautics and Space Administration Washington, D. C. 20546	Contractor
	14. SPONSORING AGENCY CODE

15. SUPPLEMENTARY NOTES

Prepared under the technical direction of the Aerospace Environment Division, Space Sciences Laboratory, NASA-Marshall Space Flight Center

16. ABSTRACT

A nine-element continuum wave spectrum, high-frequency, Doppler sounder array has been used to detect upper atmospheric wave-like disturbances during periods with severe weather activity, particularly severe thunderstorms and tornadoes. Five events of severe weather activity, including extreme tornado outbreak of April 3, 1974, were chosen for the present study. The analysis of Doppler records shows that both infrasonic waves and gravity waves were excited when severe storms appeared in the North Alabama area. Primarily, in the case of tornado activity, S-shaped Doppler fluctuations or Doppler "fold-backs" are observed, while quasi-sinusoidal fluctuations are more common in the case of thunderstorm activity. A criterion for the production of Doppler "fold-backs" is derived and compared with possible tornado conditions.

17. KEY WORDS	18. DISTRIBUTION STATEMENT
	Unclassified — Unlimited Charles A. Lundquist Director, Space Sciences Laboratory

19. SECURITY CLASSIF. (of this report)	20. SECURITY CLASSIF. (of this page)	21. NO. OF PAGES	22. PRICE
Unclassified	Unclassified	72	NTIS

TABLE OF CONTENTS

I. INTRODUCTION

The investigation of the dynamics of coupling between lower and upper atmosphere through wave generation, wave propagation and wave dissipation is essential for the understanding of the motion of the atmosphere. In particular, accurate information about atmospheric disturbances and wave propagation is required for the development of a model of the perturbed neutral atmosphere for the use in orbital/environment mission performance assessment of the Space Shuttle vehicle.

Coupling between the lower atmosphere and the ionosphere can be detected from ionospheric wave-like disturbances which are frequently observed on ground-based ionospheric sounding records as perturbations in the electron densities. Recently, Georges (1968, 1972), Baker and Davies (1969), and Davies and Jones (1972) reported observations of ionospheric wave-like disturbances which showed some correlation with severe weather activity, and suggested that infrasonic waves could be generated by the storm systems. Even though severe weather activity as possible sources of gravity-acoustic waves has been suggested, additional and more confirmative experimental evidence to support such a hypothesis is urgently necessary.

To provide more experimental evidence on the dynamics of upper atmospheric disturbances during severe weather activity, a continuous wave-spectrum, high frequency, Doppler sounder

array has been employed. The purpose of the study is to investigate the coupling between the lower and upper atmosphere (ionosphere) during severe weather activity.

Experimental observations of ionospheric wave-like disturbances during severe weather activity are from the NASA/ Marshall Space Flight Center CW Doppler sounder array located in the North Alabama region. Since January 1973, we have continuously monitored the Doppler frequency fluctuations of nine field transmitters at three stations which cover an area of 150 Km^2.

In Chapter II, we describe the characteristics of atmospheric waves. In Chapter III, experimental operations of Doppler sounder array which have been used to detect ionospheric disturbances are discussed. The procedures of data analysis from the records of Doppler fluctuations are presented in Chapter IV. In Chapter V, five events of severe thunderstorms and tornadoes, including the extreme tornado outbreak of April 3, 1974, were analyzed. In Chapter VI, we have discussed the effect of Doppler shift due to eastward wind which may affect the wave-period of acoustic-gravity waves observed during severe weather activity. Furthermore, the criterion for the excitation of S-shaped record or Doppler "fold-backs," which is very often observed during tornado activity, is derived and is compared with possible tornado conditions.

II. ATMOSPHERIC WAVES

Typical wave motions in the neutral atmosphere are the propagation of sonic waves. The normal frequency range of the sonic spectrum of the human ear is 20 Hz to 20 KHz. Based on this frequency range, the sonic waves are generally divided into the following three groups:

(1) Audio-Sonic Waves

The frequency range is within the spectrum of human ear.

(2) Ultrasonic Waves

The frequency range is above audio-sonic waves. The upper frequency limits for ultrasonic waves approach the relaxation frequencies of metals, around 10^6 MHz, beyond which materials can no longer respond to the input of mechanical wave energy.

(3) Infrasonic Waves

The frequency range is below audio-sonic waves.

In the real atmosphere, the presence of gravitational force causes the density to be vertically nonuniformly distributed which is responsible for the buoyancy oscillations of the fluid parcel of the atmosphere. The buoyancy frequency, which is also termed Brunt-Väisälä frequency, is given by

$$\omega_B = \left[\frac{g}{T}\left(\Gamma_d + \frac{dT}{dz}\right)\right]^{1/2} \qquad (2\text{-}1)$$

where g is the gravitational acceleration; T, the temperature, z, the spatial coordinate along the vertical height; and Γ_d, the dry adiabatic lapse rate which is defined

$$\Gamma_d = \frac{g}{R}\left(\frac{\gamma-1}{\gamma}\right) . \qquad (2\text{-}2)$$

Here R is the universal gas constant and $\gamma = C_p/C_v$ where C_p is the specific heat at constant pressure, and C_v is the specific heat. The height variations of molecular temperature T, sound speed a, ratio of specific heat γ, and Brunt-Väisälä wave period τ_B ($\equiv 2\pi/\omega_B$) are given in Figures 1, 2, 3 and 4, respectively. It can be seen from Figure 4 that the Brunt-Väisälä frequency is practically less than 0.05 Hz in the atmosphere and it is therefore more convenient to speak of the period of the wave. This characteristic frequency caused by the buoyancy force is so small, as the period is several minutes to more than ten minutes in real atmosphere. Thus, only comparable low frequency waves would be affected by the buoyancy force. It is for this reason that the waves modified by the buoyancy force are limited to infrasonic waves in the atmosphere. In fact, the modification is so drastic that the resulting waves are called acoustic-gravity waves.

The characteristics of acoustic-gravity waves can be shown in simple calculations. To do so, the atmosphere is

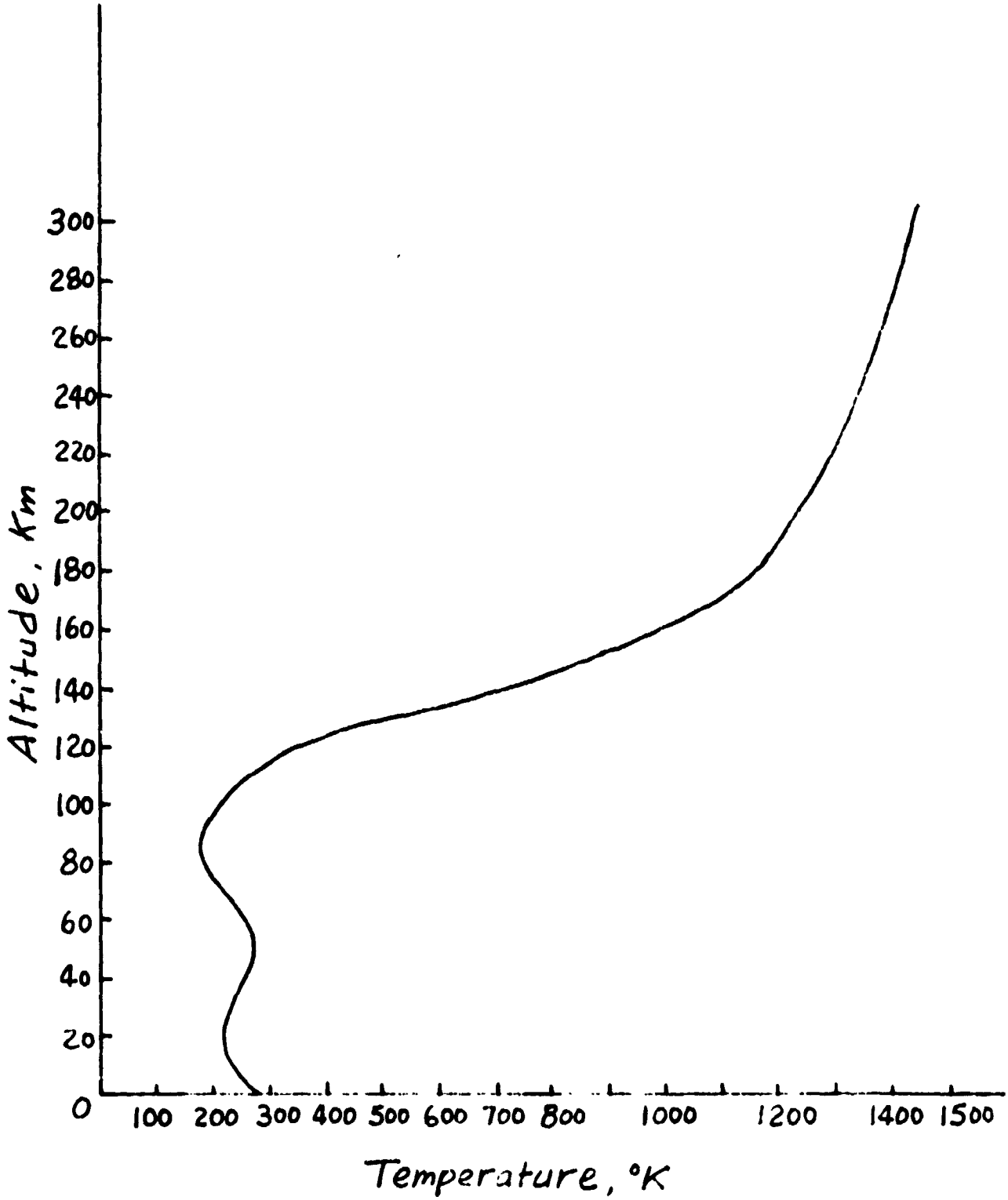

Figure 1. The height variation of molecular temperature in real atmosphere.

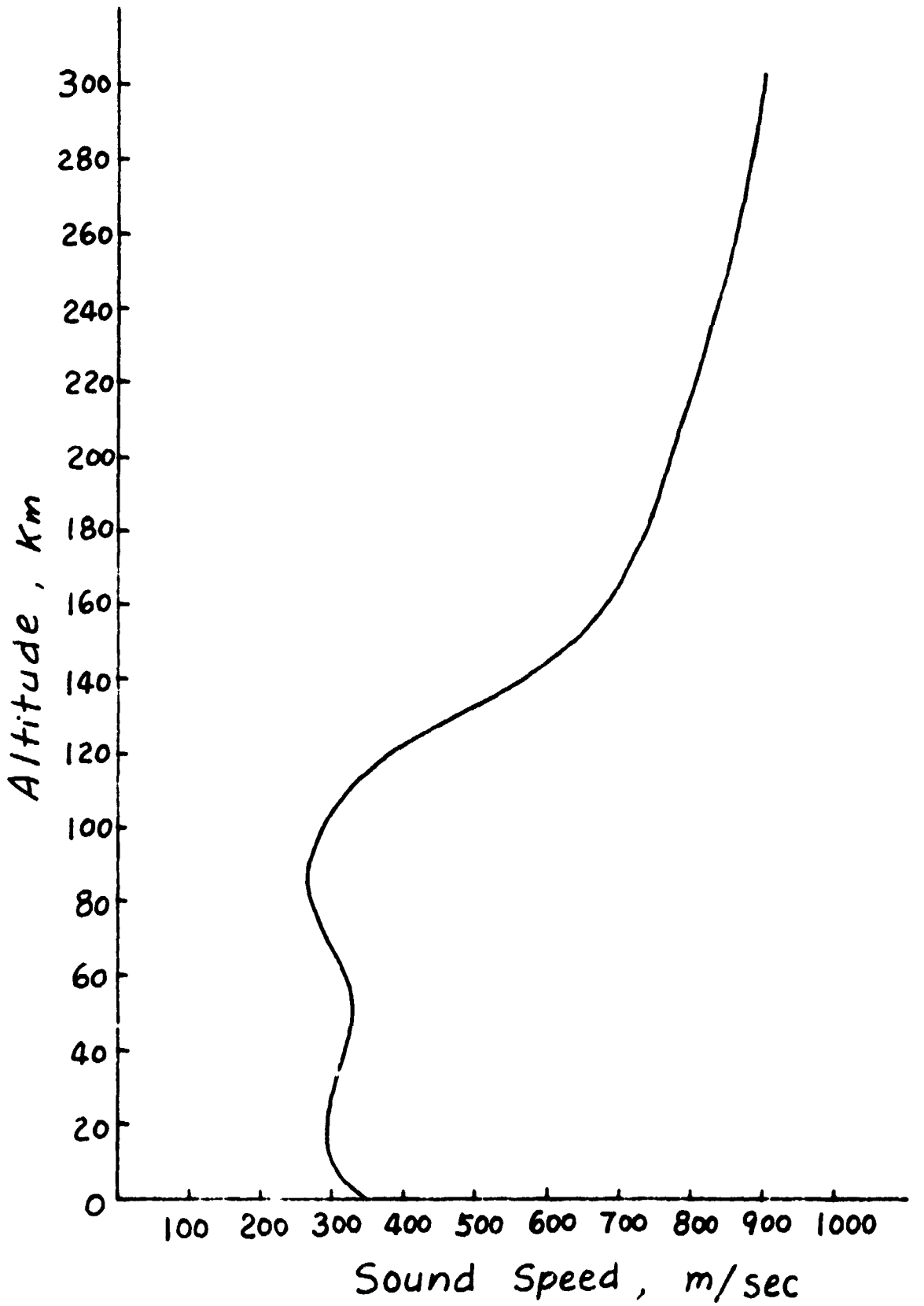

Figure 2. The height variation of sound speed in real atmosphere.

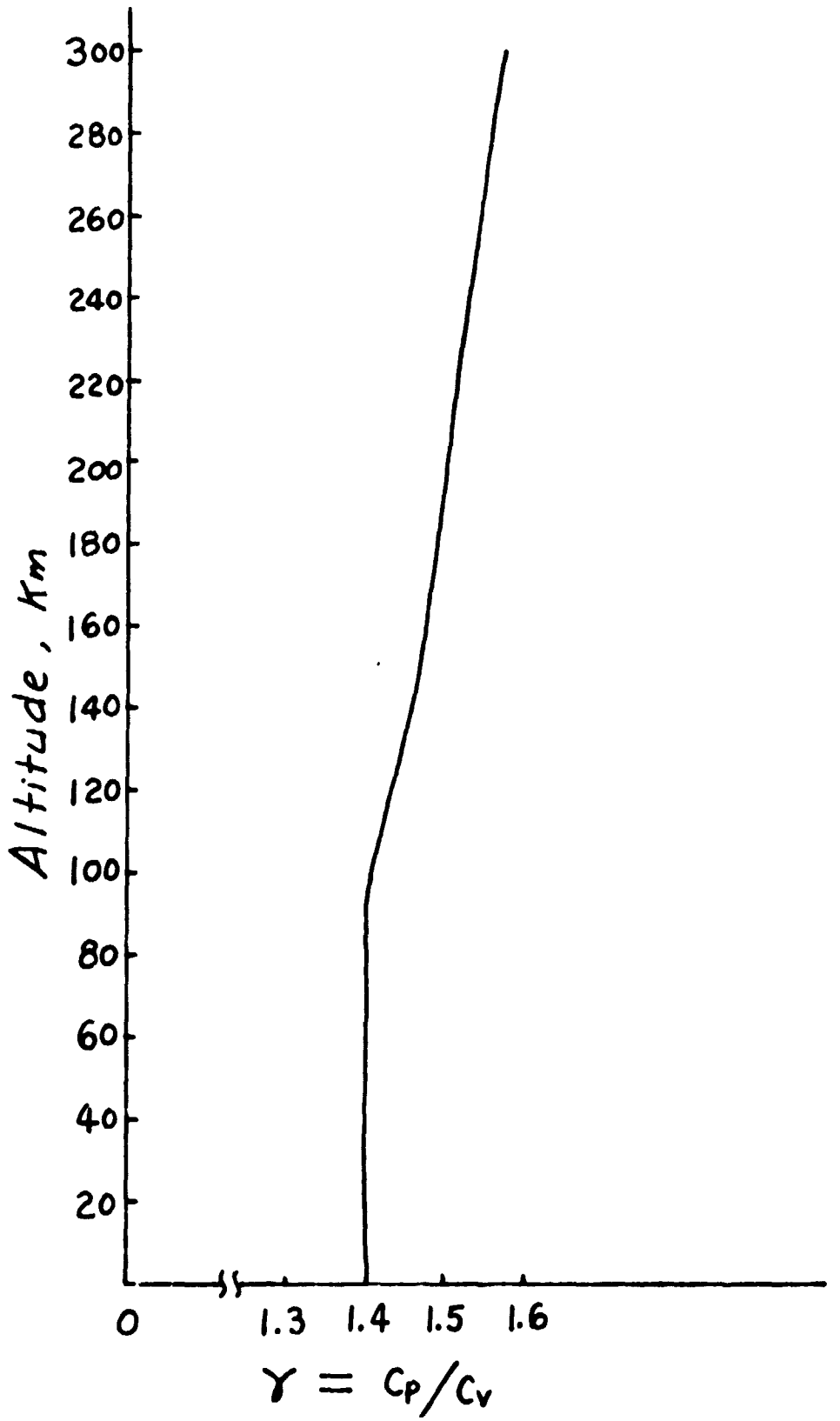

Figure 3. The height variation of ratio of specific heat γ in real atmosphere.

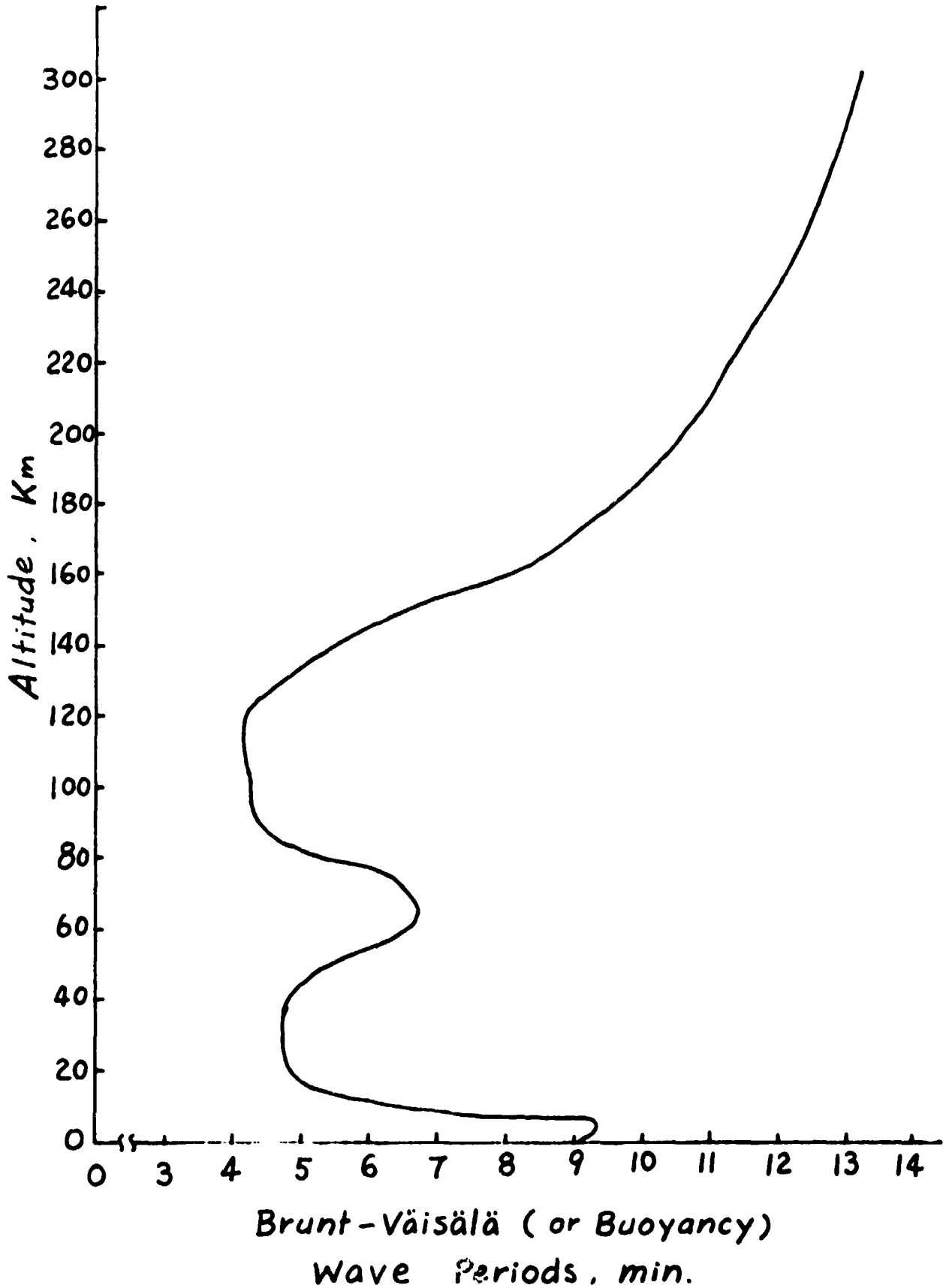

Figure 4. The height variation of buoyancy or Brunt-Väisälä wave-period in real atmosphere.

assumed to be nonrotating (for a wave period shorter than two hours) with no large-scale neutral wind. The equations are the equation of continuity, the equation of motion, and the equation of energy which are replaced by the adiabatic equation in this case, namely,

$$\frac{\partial \rho}{\partial t} + \underset{\sim}{\nabla} \cdot (\rho \underset{\sim}{v}) = 0 \tag{2-3}$$

$$\rho \frac{D\underset{\sim}{v}}{Dt} = - \underset{\sim}{\nabla} P + \rho \underset{\sim}{g} \tag{2-4}$$

$$\frac{DP}{Dt} = a^2 \frac{D\rho}{Dt} \tag{2-5}$$

where the convective derivative is $D/Dt = \partial/\partial t + \underset{\sim}{V} \cdot \underset{\sim}{\nabla}$. Here ρ denotes mass density; $\underset{\sim}{V}$, velocity; P, pressure; $a = (\partial P/\partial \rho)^{1/2}_{ad.a}$, sonic velocity; and $\underset{\sim}{g} = (0, 0, -g)$, gravitational acceleration. For a static, motionless, isothermal atmosphere the mass density must be distributed exponentially as a function of height

$$\langle \rho \rangle = \rho_o \, e^{-z/H} \tag{2-6}$$

where ρ_o is the density at $z = 0$, and $H = a^2/\gamma g$ (γ is the ratio of constant pressure specific heat to constant volume specific heat). The corresponding pressure distribution is

$$\langle p \rangle = P_o \, e^{-z/H} \, . \tag{2-7}$$

Let the isothermal atmosphere be perturbed according to the following scheme:

$$\begin{bmatrix} \rho(\underset{\sim}{r}, t) \\ P(\underset{\sim}{r}, t) \\ \underset{\sim}{V}(\underset{\sim}{r}, t) \end{bmatrix} = \begin{bmatrix} <\rho(z)> + \delta\rho(\underset{\sim}{r}, t) \\ <P(z)> + \delta P(\underset{\sim}{r}, t) \\ \delta\underset{\sim}{V}(\underset{\sim}{r}, t) \end{bmatrix} \tag{2-8}$$

where < > denotes the equilibrium quantities and δ implies the perturbations. After linearizing the equations, and assuming that the perturbation is proportional to

$$\exp i\,(\omega t - \underset{\sim}{k} \cdot \underset{\sim}{r})$$

we have the following dispersion relation

$$\frac{k_x^2}{(1-\omega_a^2/\omega^2)/(1-\omega_b^2/\omega^2)} + \frac{k_z^2}{1-\omega_a^2/\omega^2} = k_o^2 \tag{2-9}$$

where $k_o = \omega/a$; $\omega_a = \gamma g/2a = a/2H$ = acoustic cutoff frequency; and $\omega_b = (\gamma-1)^{1/2}\, g/a$ = buoyancy frequency at isothermal atmosphere, namely,

$$\omega_b = \omega_B\Big]_{\frac{dT}{dz} \to 0} \tag{2-10}$$

Let us discuss the properties of the dispersion relation (2-9) in the following three different ranges:

(1) $\underline{\omega < \omega_b}$

This is gravity wave. The phase velocity of gravity waves is always less than the velocity of sound waves.

(2) $\underline{\omega_b < \omega < \omega_a}$

This is cutoff region where no acoustic-gravity

waves exist under the condition of isothermal atmosphere.

(3) $\omega > \omega_a$

This is acoustic wave. The phase velocity of acoustic waves is equal or greater than the velocity of sound waves.

In the real atmosphere, the assumption of isothermal atmosphere is no longer valid. This implies that the cutoff region of the form discussed for isothermal atmosphere no longer exists. Therefore, the overlap between the regions of acoustic waves and gravity waves will be expected.

III. EXPERIMENTAL OPERATIONS

The continuous wave-spectra Doppler sounder array was developed by Davies (1962). Davies and Baker (1966) gave a description of the theory and an interpretation of the data. NASA/Marshall Space Flight Center CW Doppler sounder array consists of three sites with nine field transmitters operating at 4.0125, 4.759 and 5.734 MHz with receivers located at NASA/Marshall Space Flight Center (NASA/MSFC), Alabama (see Figure 5 for map description). The geographic locations of the field transmitters are shown in Table 1. The received signals from all nine transmitters are mixed with stable oscillators of the same nominal frequencies, but are offset several Hz higher. The beat frequencies are then recorded on a slowly moving (one inch per minute) magnetic tape. For data analysis, the tapes are played back at higher speeds into an audio spectrum analyzer. The output of the spectrum analyzer is connected to a facsimile recorder which gives a strip chart record of the Doppler shifted frequency components against time.

A block diagram of the equipment for one transmitting station is shown in Figure 6. Three ovenized crystal oscillators are built into one chassis, as shown in the block diagram of Figure 7. Since each of the three transmitters must be slightly different so they can be distinguished from

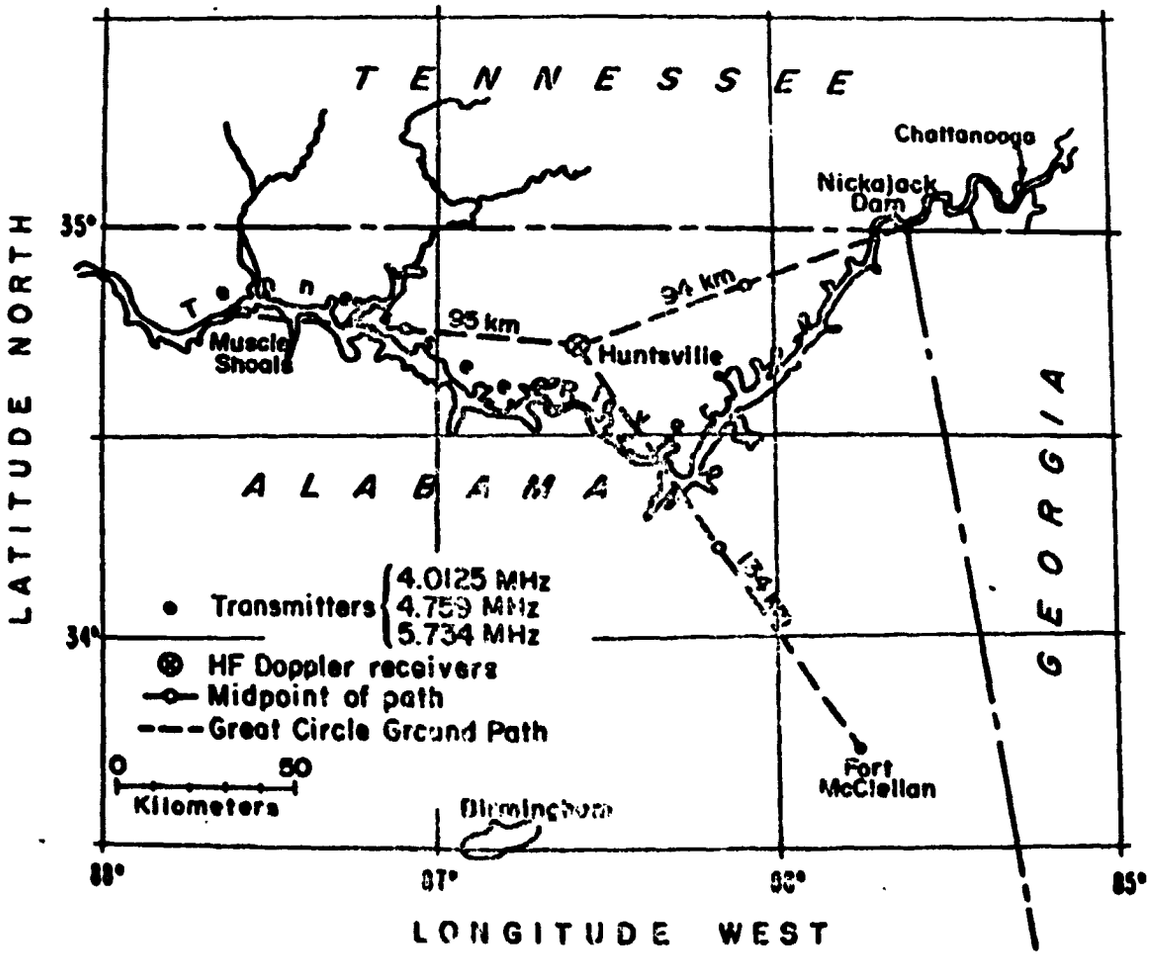

Figure 5. Locations of three sites of field transmitters and receivers of NASA/Marshall Space Flight Center Continuous wave spectrum, high frequency Doppler sounder array system.

TABLE 1

Geographic Location of the CW Doppler Sounder Array

Station	Latitude	Longitude
NASA/MSFC, Alabama	34° 39'N	86° 40'W
Ft. McClellan, Alabama	33° 44'N	85° 48'W
TVA Muscle Shoals, Alabama	34° 46'N	85° 38'W
TVA Nickajack Dam, Tennessee	35° 01'N	87° 38'W

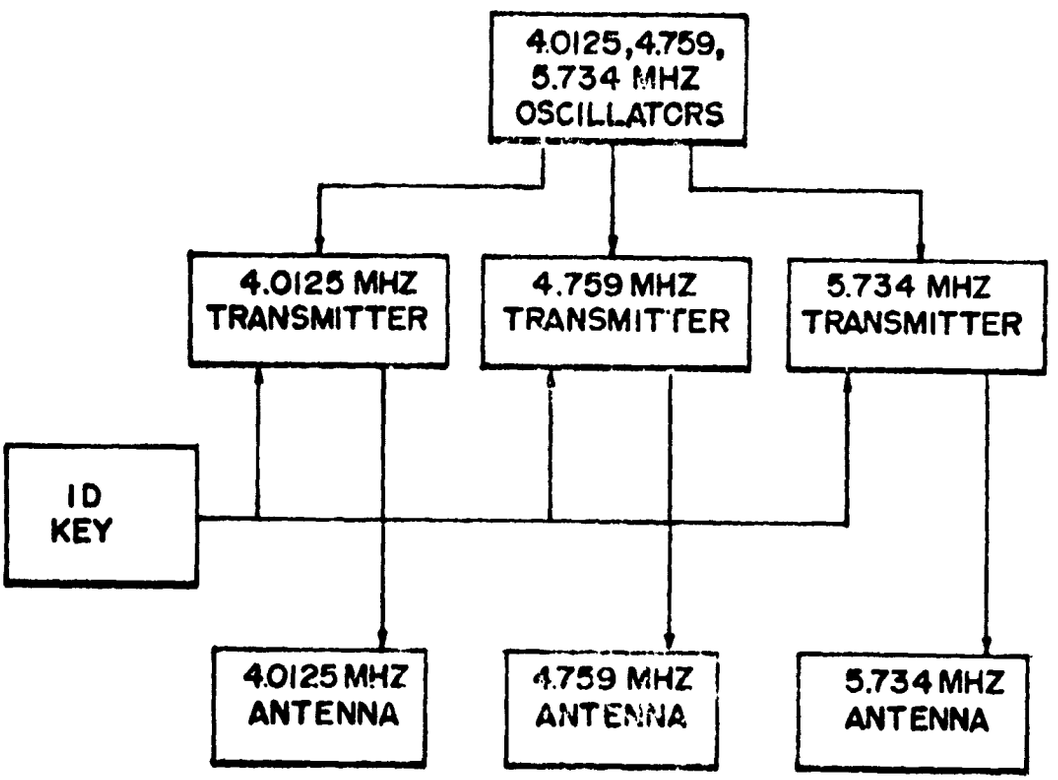

Figure 6. Block diagram of transmitting system.

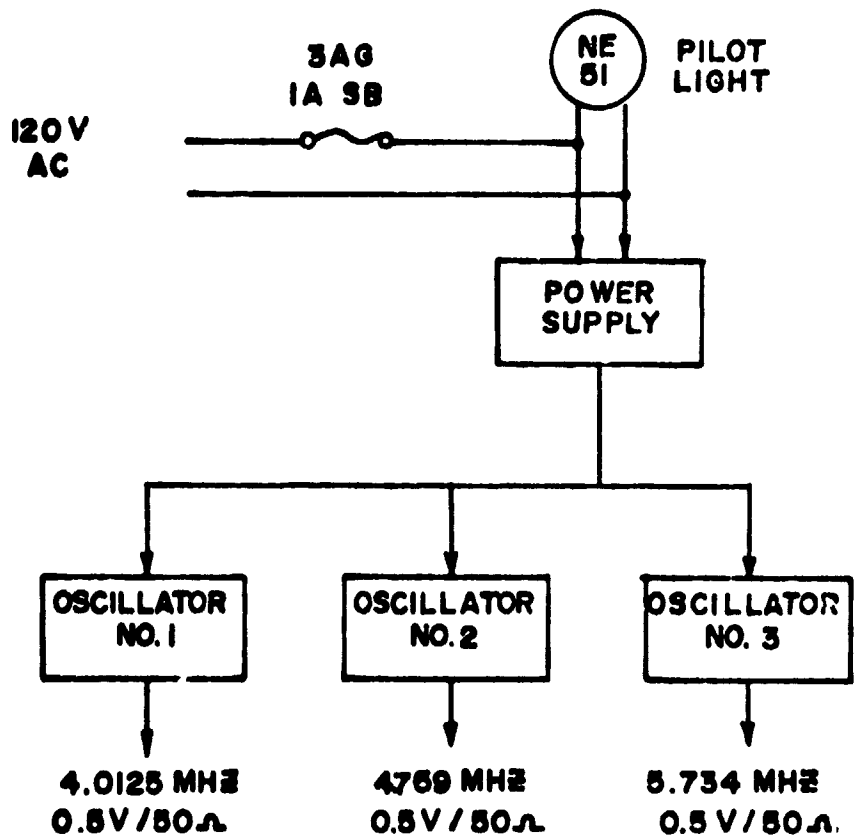

Figure 7. Block diagram of Oscillator chasis.

each other at the receiver. The actual frequencies for the field transmitters have been set as in Table 2. At the receiving station, the oscillators have been set exactly at the nominal frequencies so that in the absence of Doppler variations, the offsets of the transmitter oscillators are equal to the beat frequencies.

The transmitters are modified versions of the Heathkit DK 60B. The transmitting antennas are halfwave dipoles. In order to maximize vertical radiation and minimize horizontal radiation, the height of the dipoles above ground should be between one-eighth to one-fourth wavelength. Since all three antenna at a site are in one array, a height of approximately 30 feet has proven to be practical. To null the horizontal radiation in the direction of the receiver, the transmitting antenna at the sites are oriented so that the array is broadside to the receiving site and the ends of the antenna point to the receiver site (NASA/MSFC). Ground waves are not expected to be a problem since the sites are farther than 40 Km from the receivers. If a ground wave is received, it can be identified by its stable beat frequency on the Doppler records.

A block diagram of the receiving and recording system is shown in Figure 8. The reflected ionospheric echoes from the nine field transmitters are received by three Hammarlund SP-600-JX-17 communication receivers at three different nominal frequencies. These receivers use single conversion for channel

Table 2

Nominal and Actual Operating Frequencies of Nine Transmitters of NASA/Marshall Space Flight Center Doppler Sounder Array System

Nominal Frequency	Actual Frequencies		
	Three Transmitters at Muscle Shoals, Alabama	Three Transmitters at Nickajack Dam, Tennessee	Three Transmitters at Ft. McClellan, Alabama
4.0125 MHz	4.0125 MHz + 10 Hz	4.0125 MHz + 20 Hz	4.0125 MHz + 30 Hz
4.759 MHz	4.759 MHz + 10 Hz	4.759 MHz + 20 Hz	4.759 MHz + 30 Hz
5.734 MHz	5.734 MHz + 10 Hz	5.734 MHz + 20 Hz	5.734 MHz + 30 Hz

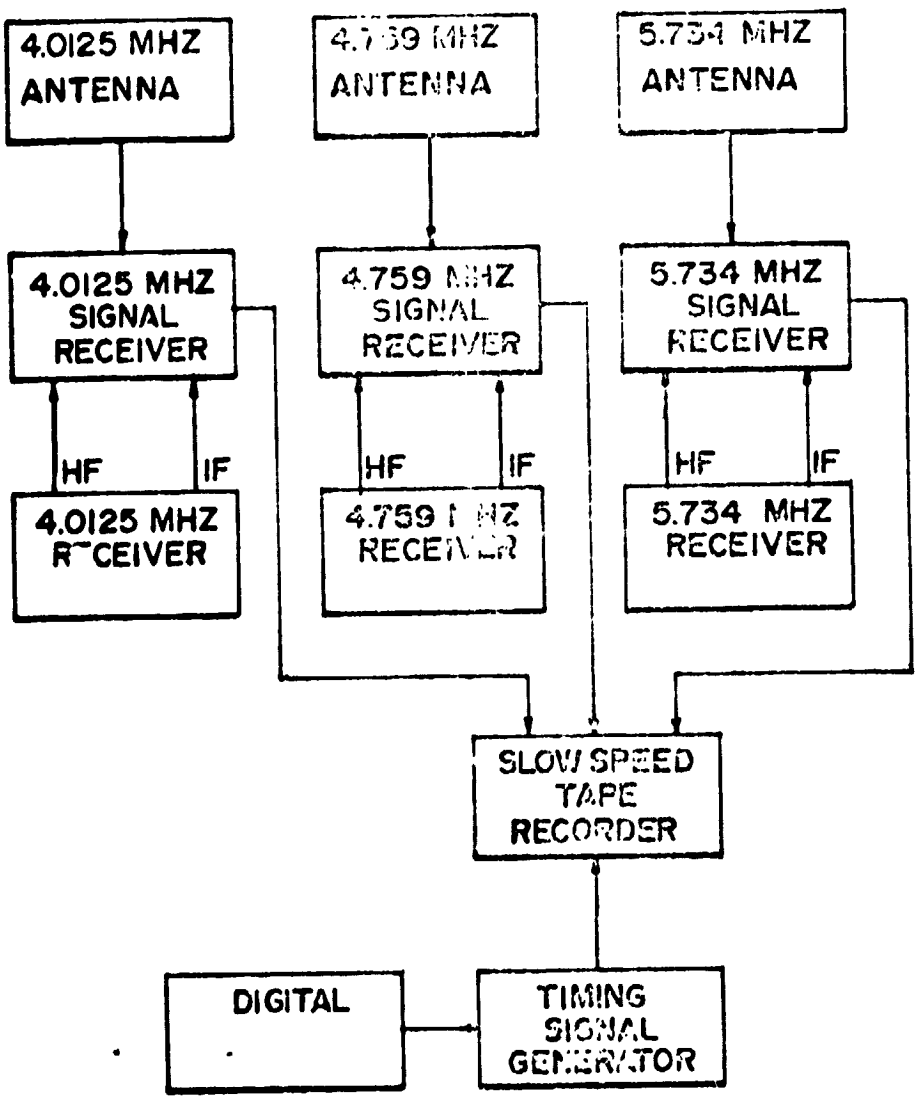

Figure 8. Block diagram of receiving system.

frequencies below 7.4 MHz, and double conversion above 7.4 MHz. In either case, the internal crystal HF oscillator is used instead of the variable frequency oscillator. It is not necessary that the HF oscillator in the signal receiver has the stability of the reference receiver to be mixed with the signal from the reference oscillator. Thus, any variations in frequency disappear when the signal intermediate frequency (IF) is mixed with the reference IF.

In order to obtain the accurate timing of ionospheric disturbances, a time code is recorded on channel 4 of the data tape. When the tape is played back for spectrum analysis, the channel 4 output is mixed with whichever data channel is being played back, so that data and timing appear simultaneously on the records. In other words, channels 1, 2 and 3 are used for data, with a timing signal recorded on channel 4. The data tapes are played back on a four channel tape recorder at a speed of 15 inches per second. Each data tape is played back three times, with each playback, one data channel is mixed with the timing channel. The channels are recorded as follows:

Channel 1: 4.0125 MHz, low frequency

Channel 2: 4.759 MHz, middle frequency

Channel 3: 5.734 MHz high frequency

Channel 4: Timing signal.

The output from the tape recorder is spectrum analyzed using a Federal Scientific UA-6B, Ubiguitous audio spectrum analyzer. The output from the spectrum analyzer is fed to a

Gift GPR facsimile recorder which gives a record of frequency against time.

In the present study, we are interested in the analysis of atmospheric waves generated by severe weather activity. A few examples during severe weather activity, particularly thunderstorms and tornadoes, have been chosen for data analysis. The procedures of data analysis will be discussed in the following sections.

IV. PROCEDURES OF DATA ANALYSIS

The visible record of the Doppler data is obtained by frequency analysis of the signal. The frequency analysis is carried out by using a UA6B Ubiguitous audio spectrum analyzer. The output from the spectrum analyzer is displaced on a facsimile chart. In the present study, we are particularly interested in the investigation of the specific atmospheric-ionospheric coupling during thunderstorm and tornado activity which can be identified on the Doppler record. After visual identification of the events due to severe storm activity, the segments of the data tape containing the events are played back at a slower speed for better time resolution. By playing back the tapes at a slower speed and recording the data, one can achieve a time resolution of about five seconds, depending on the time-scale of interest, to study the fine structure in the Doppler variation.

The Doppler fluctuations printed in facsimile chart by playing back the tapes are then subjected to numerical digitizing. The digitized data will be used to determine time displacement and wave frequency of the fluctuations. In other words, for a given sample of the Doppler sounder record, the time displacements are determined by computing the cross-correlation functions. Consider two time series functions given by $x_\alpha(t)$ and $x_\beta(t)$. The cross-correlation function is given by

$$C_{\alpha\beta}(\tau) = \lim_{T\to\infty} \frac{1}{2T} \int_{-T}^{T} x_\alpha(t)\, x_\beta(t+\tau)\,dt \qquad (4.1)$$

where τ is the time lag, or the time displacement between the two functions being correlated. In a special case when $x_\alpha = x_\beta$, Equation (4.1) becomes the auto correlation function

$$C_{\alpha\alpha}(\tau) = \lim_{T\to\infty} \frac{1}{2T} \int_{-T}^{T} x_\alpha(t)\, x_\alpha(t+\tau)\,dt \qquad (4.2)$$

In general, the correlation matrix [C] can be expressed by

$$[C] = \begin{bmatrix} C_{11}(\tau) & C_{12}(\tau) & C_{13}(\tau) \\ C_{21}(\tau) & C_{22}(\tau) & C_{23}(\tau) \\ C_{31}(\tau) & C_{32}(\tau) & C_{33}(\tau) \end{bmatrix} \qquad (4.3)$$

In our case, if M, N and F refer to the ionospheric reflection points to the transmitters located at Muscle Shoals, Alabama; Nickajack Dam, Tennessee; and Fort McClellan, Alabama to the receivers at NASA/MSFC, respectively, the correlation Matrix becomes

$$[C] = \begin{bmatrix} C_{MM}(\tau) & C_{MN}(\tau) & C_{MF}(\tau) \\ C_{NM}(\tau) & C_{NN}(\tau) & C_{NF}(\tau) \\ C_{FM}(\tau) & C_{FN}(\tau) & C_{FF}(\tau) \end{bmatrix}. \qquad (4.4)$$

The power spectral density and cross power spectral density are obtained by Fourier transforming the auto and cross correlation functions, respectively, i.e.,

$$P_{\alpha\alpha}(\omega) = \frac{1}{2\pi} \int_{-\infty}^{\infty} C_{\alpha\alpha}(\tau)\, e^{-i\omega\tau}\, d\tau \qquad (4.5)$$

and

$$P_{\alpha\beta}(\omega) = \frac{1}{2\pi} \int_{-\infty}^{\infty} C_{\alpha\beta}(\tau)\, e^{-i\omega\tau}\, d\tau \qquad (4.6)$$

where $\omega = 2\pi f$ is the angular frequency in radian/sec and f is frequency in Hz. In general, the cross-power spectral density is complex,

$$P_{\alpha\beta}(\omega) = P^{r}_{\alpha\beta}(\omega) + i\, P^{i}_{\alpha\beta}(\omega) \qquad (4.7)$$

where $P^{r}_{\alpha\beta}(\omega)$ is the real part and $P^{i}_{\alpha\beta}$ is the imaginary part of the cross spectrum function. The phase density spectrum can be obtained from

$$\theta(\omega) = \theta_{\beta}(\omega) - \theta_{\alpha}(\omega)$$

$$= \tan^{-1}\left[\frac{P^{i}_{\alpha\beta}(\omega)}{P^{r}_{\alpha\beta}(\omega)}\right] \qquad (4.8)$$

where $\theta_{\alpha}(\omega)$ is phase of time series $x_{\alpha}(t)$, and $\theta_{\beta}(\omega)$ is phase of time series $x_{\beta}(\omega)$. The magnitude of the complex continuous spectrum, called the amplitude density spectrum, is

$$\left|P_{\alpha\beta}(\omega)\right| = \left\{ [P^{r}_{\alpha\beta}(\omega)]^2 + [P^{i}_{\alpha\beta}(\omega)]^2 \right\}^{1/2} \qquad (4.9)$$

The power can be calculated from the integration of power spectral density

$$W = \int_{\omega_1}^{\omega_2} P_{\alpha\alpha}(\omega)\, d\omega \qquad (4.10)$$

The coherence estimates are given by

$$\gamma(\omega) = \frac{P_{\alpha\beta}(\omega)}{[P_{\alpha\alpha}(\omega)\ P_{\beta\beta}(\omega)]^{1/2}} \qquad (4.11)$$

where $\gamma(\omega)$ is the complex coherence. The amplitude of the cross spectrum at each frequency is the product of the corresponding amplitudes in the two time series. If a particular spectral component is absent from either time series, then it will be absent in the cross-spectrum and the coherence will be minimum at that frequency.

In our case the frequency of the ionospheric disturbances caused by severe weather activity can be computed from both power spectral density and cross spectral density. The time delay between the reflection points can be obtained from cross-correlation function. Let τ_{MN} and τ_{MF} be the time delays between the reflection points M-N and M-F, respectively; and D_{MN} and D_{MF} be the distance between the similar points, respectively. The apparant trace velocities V_{MN} and V_{MF} are given by the following relations (See Figure 9):

$$V_{MN} = \frac{D_{MN}}{\tau_{MN}} \quad \text{and} \quad V_{MF} = \frac{D_{MF}}{\tau_{MF}} \qquad (4.12)$$

The magnitude horizontal trace velocity V_H and the direction ϕ (measured east from north) can be determined from the following set of equations:

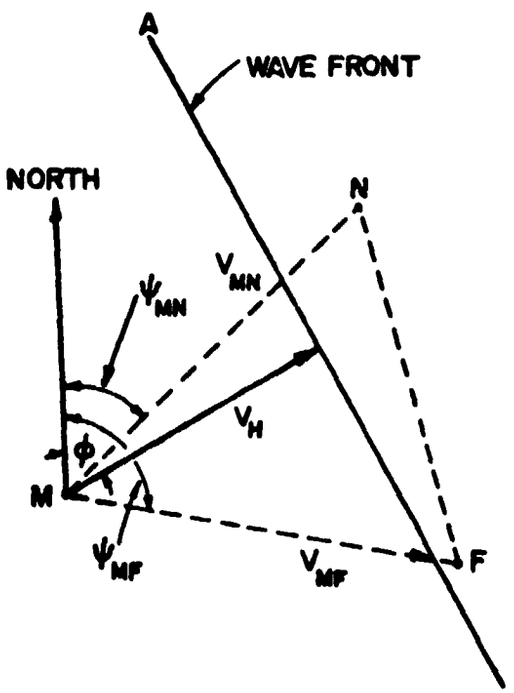

Figure 9. Graphical representation of wave front moving across the doppler sounder array.

$$\text{Cot } \phi = - \frac{V_{MN} \text{ Sin } \psi_{MN} - V_{MF} \text{ Sin } \psi_{MF}}{V_{MN} \text{ Cos } \psi_{MN} - V_{MF} \text{ Cos } \psi_{MF}} \qquad (4.13)$$

and the magnitude of V_H is given by

$$V_H^2 = \frac{V_{MN}^2 \, V_{MF}^2 \, \text{Sin}^2 \, (\psi_{MN} - \psi_{MF})}{V_{MN}^2 + V_{MF}^2 - 2 \, V_{MN} \, V_{MF} \, \cos \, (\psi_{MN} - \psi_{MF})} \qquad (4.14)$$

where ψ_{MN} and ψ_{MF} and the angles between the geographic north and lines MN and MF, respectively. The true velocity may be determined by computing the vertical trace velocity V_v. The vertical trace velocity V_v may be determined from the time displacements at various frequencies and the difference of reflection points for a given transmitter and receiver location, are assumed to lie on a vertical plane. The heights of reflections for various frequencies involved are determined from the ionogram analysis. From the values of horizontal phase velocity V_H and vertical trace velocity V_v, the true phase velocity may be determined as shown in Figure 10.

Fortran listing of computer program for the computation of cross correlation functions, auto correlation functions, power spectral density, cross power spectral density, cross spectral amplitudes, cross spectral phases, cross spectral coherences, etc., are included in the appendix.

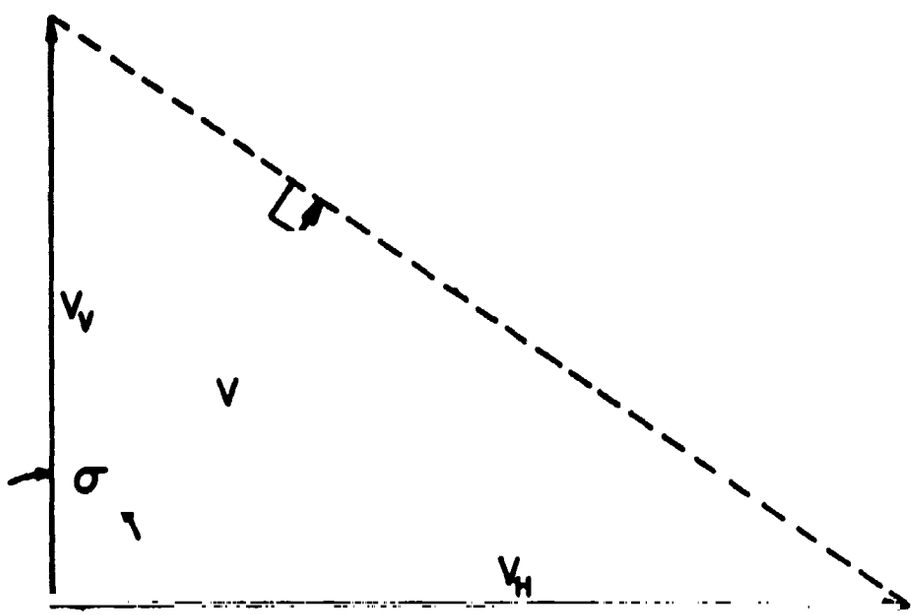

Figure 10. Graphical representation for computing phase velocity of the wave front.

V. GENERATION OF ACOUSTIC GRAVITY WAVES BY SEVERE WEATHER ACTIVITY

In this section, we present the experimental evidence of wavelike disturbances in the ionosphere caused by severe weather activity, particularly due to thunderstorms and tornadoes. The atmospheric waves observed in the ionospheric height are in the category of acoustic-gravity waves. As described in Section III and Section IV, the data obtained from the Doppler sounder are then subjected to power spectrum and cross power spectrum analyses. The results of experimental evidence is shown as follows:

A. Thunderstorm Observation

Two thunderstorm events of May 26, 1973 and March 20, 1974, have been chosen and discussed here.

(1) May 26, 1973

The Doppler record for this event is shown in Figure 11 at an operating radio frequency of 4.0125 MHz. It is evident in this figure that the Doppler fluctuations are highly disturbed until 1100 CDT. Both power spectrum density and cross power spectrum density analyses indicates that the periodicity of the Doppler frequency fluctuations are in the 3 to 5 minute range. The magnitude of the horizontal phase velocities obtained from the cross power spectrum

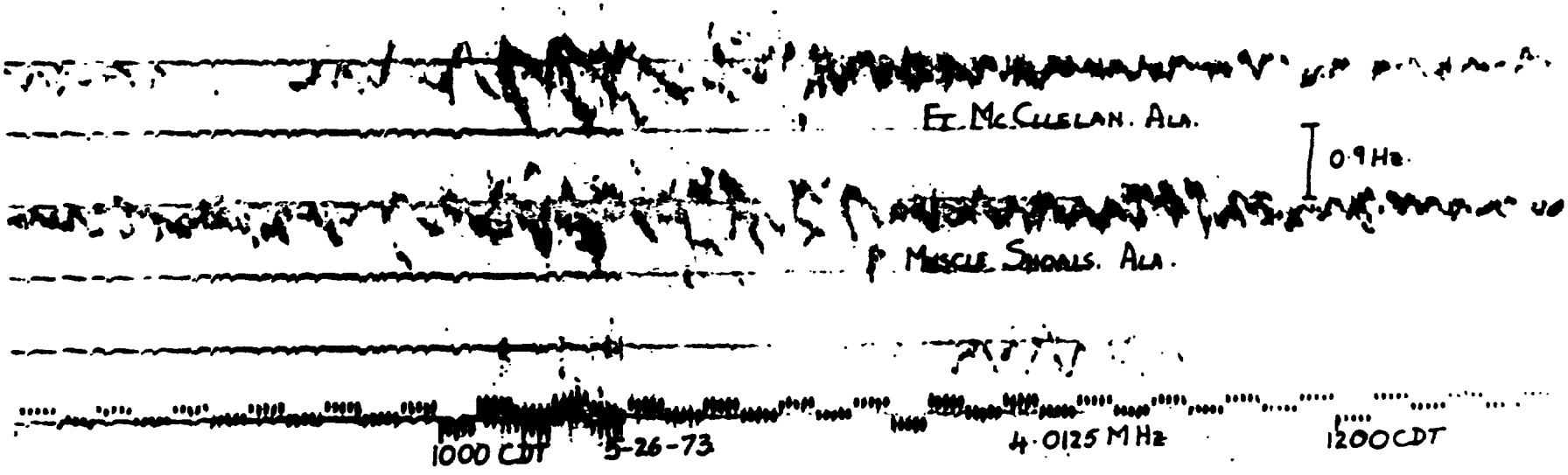

Figure 11. CW Doppler record at the operating frequency of 4.0125 MHz (event on May 26, 1973).

density analysis or cross-correlogram is shown to be 1000 m/sec propagating from the south and southwest.

(2) May 20, 1974

Figures 12, 13 and 14 are the CW Doppler records at operating frequencies 4.0125, 4.759 and 5.734 MHz, respectively, under thunderstorm conditions of March 20, 1974. No tornadoes were sighted in or around North Alabama on this day; therefore, it can be classified as a severe thunderstorm active day. The thunderstorm associated disturbances are clearly shown on all the records beginning at 1610 CDT and continuing through the early morning hours. Wavelike fluctuations with long periods of 4 to 5.5 minutes are clearly shown on the 4.0125 MHz record beginning at 2200 CDT and lasting through 0300 CDT. At higher operation frequencies, namely 4.759 and 5.734 MHz, the ionospheric reflected signal was lost after 2300 CDT. The CW Doppler records of March 20, 1974, were subjected to cross correlation analysis to compute the phase velocities. The horizontal trace velocities showed a magnitude of 1000 m/sec propagating from a direction southwest of the Doppler sounder. Examination of the Doppler sounder records also reveals that the frequency fluctuations have a constant amplitude and that they persisted for 4 to 5 hours.

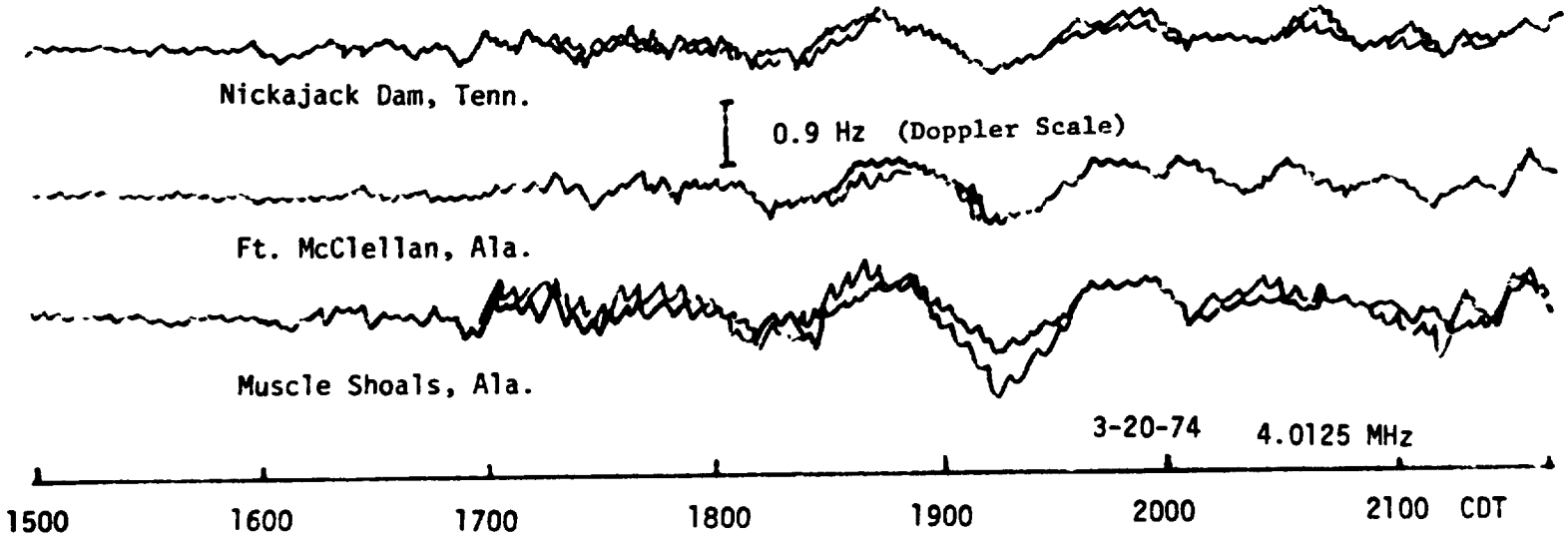

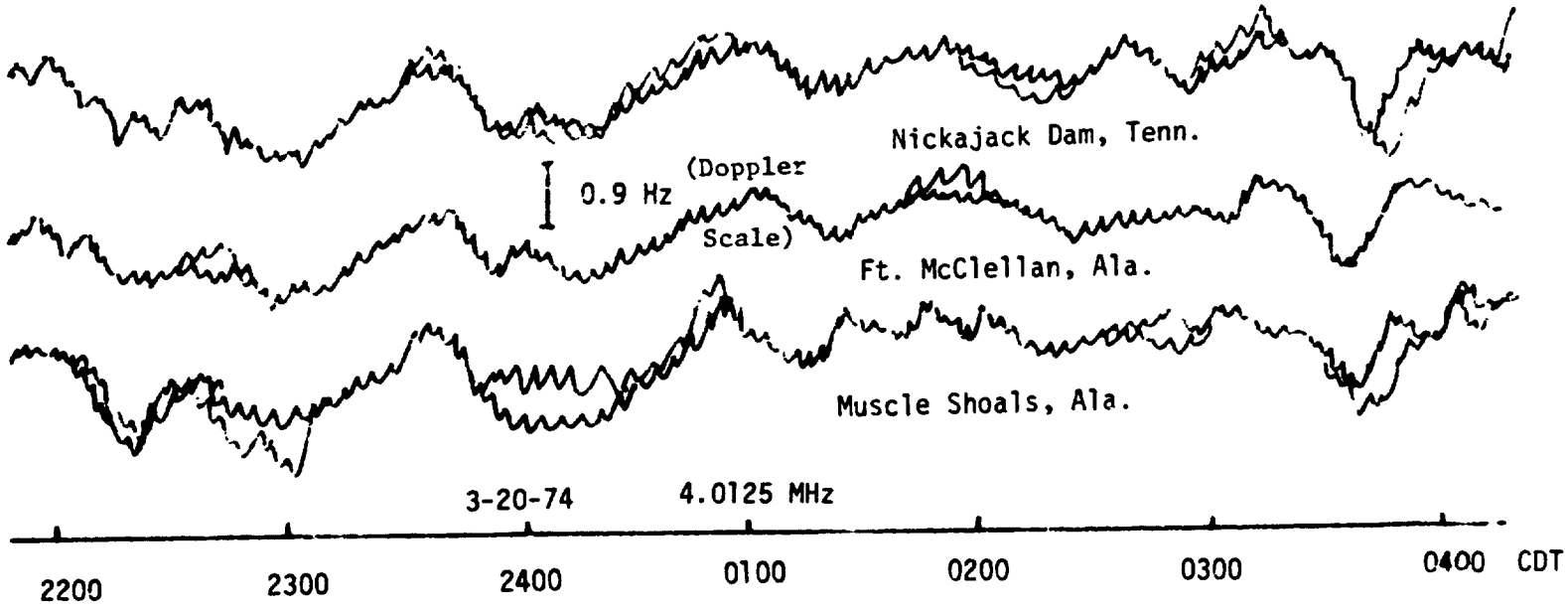

Figure 12. CW Doppler record at the operating frequency of 4.0125 MHz (event on March 20, 1974).

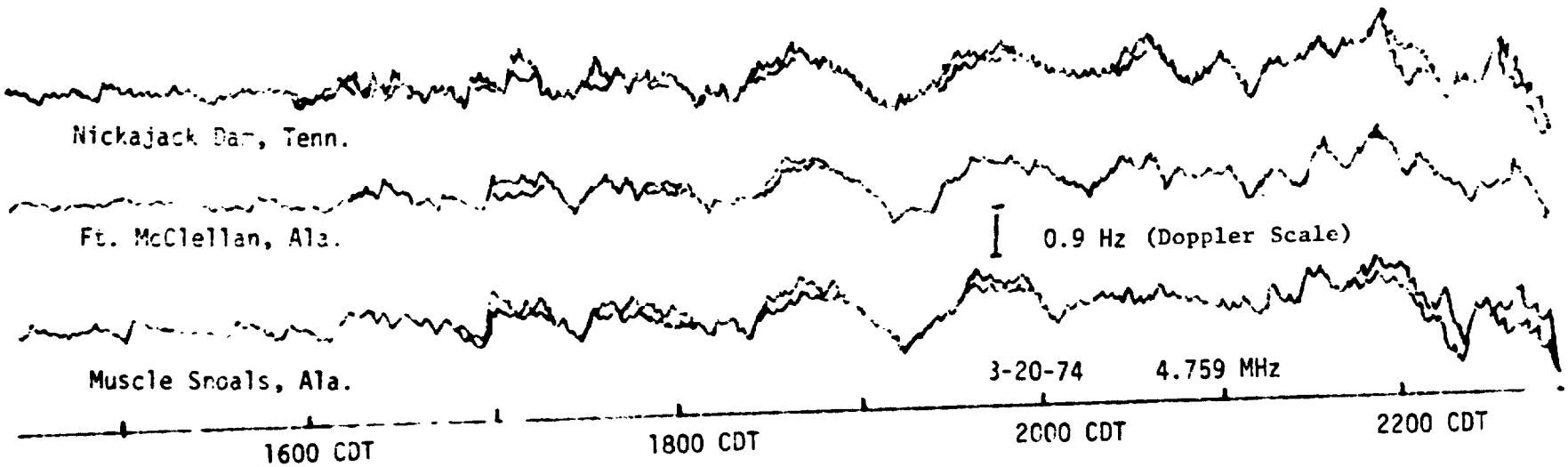

Figure 13. CW Doppler record at the operating frequency of 4.759 MHz (event on March 20, 1974).

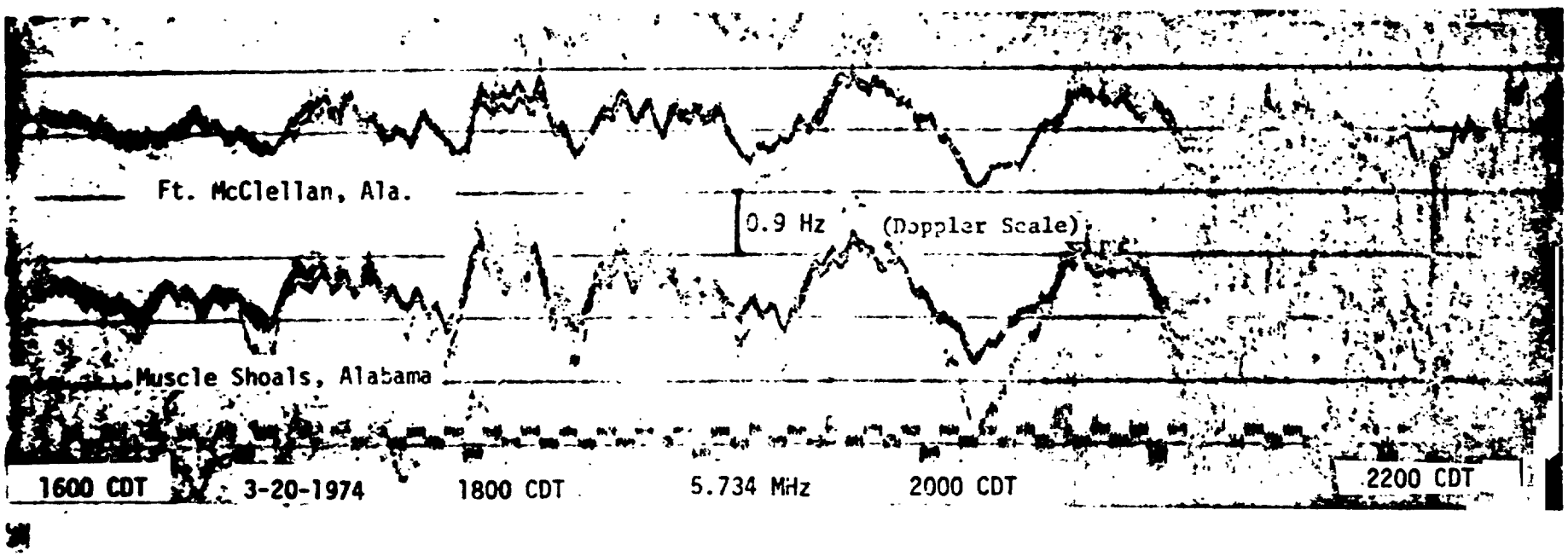

Figure 14. CW Doppler record at the operating frequency of 5.743 MHz (event on March 20, 1974).

B. Tornado Observation

The three tornado events of November 20, 1973, November 27, 1973 and the extreme tornado outbreak of April 3, 1974 have been chosen and discussed in this report.

(1) November 20, 1973

Figures 15 and 16 show a CW Doppler record for November 20, 1973, at the operating frequencies of 4.0125 MHz, and 4.759 and 5.734 MHz, respectively. The wave-like fluctuations are clearly seen beginning at 1230 CST and continuing through the evening. The periodicity of these wave-like disturbances based on the analyses from power spectrum and cross power spectrum is shown to be in the 6 to 8 minute range. The phase velocities of the disturbances, derived from a cross correlation analysis, are propagating from the south-west with a magnitude of 600-700 m/sec. The Doppler record of November 20, 1973, is expanded on the time axis to clearly show the time variations (Figure 17). It can be seen from Figure 17 that the Doppler fluctuations are not quasi-sinusoidal but are S-type waves with several Doppler fold backs. Radar weather summary charts for November 20, 1973 are shown in Figure 18. The weather map clearly shows the areas of radar echoes, lines of radar echoes and heights of echo tops. The lines of radar echoes are from the southwest to the north of the Doppler system. The

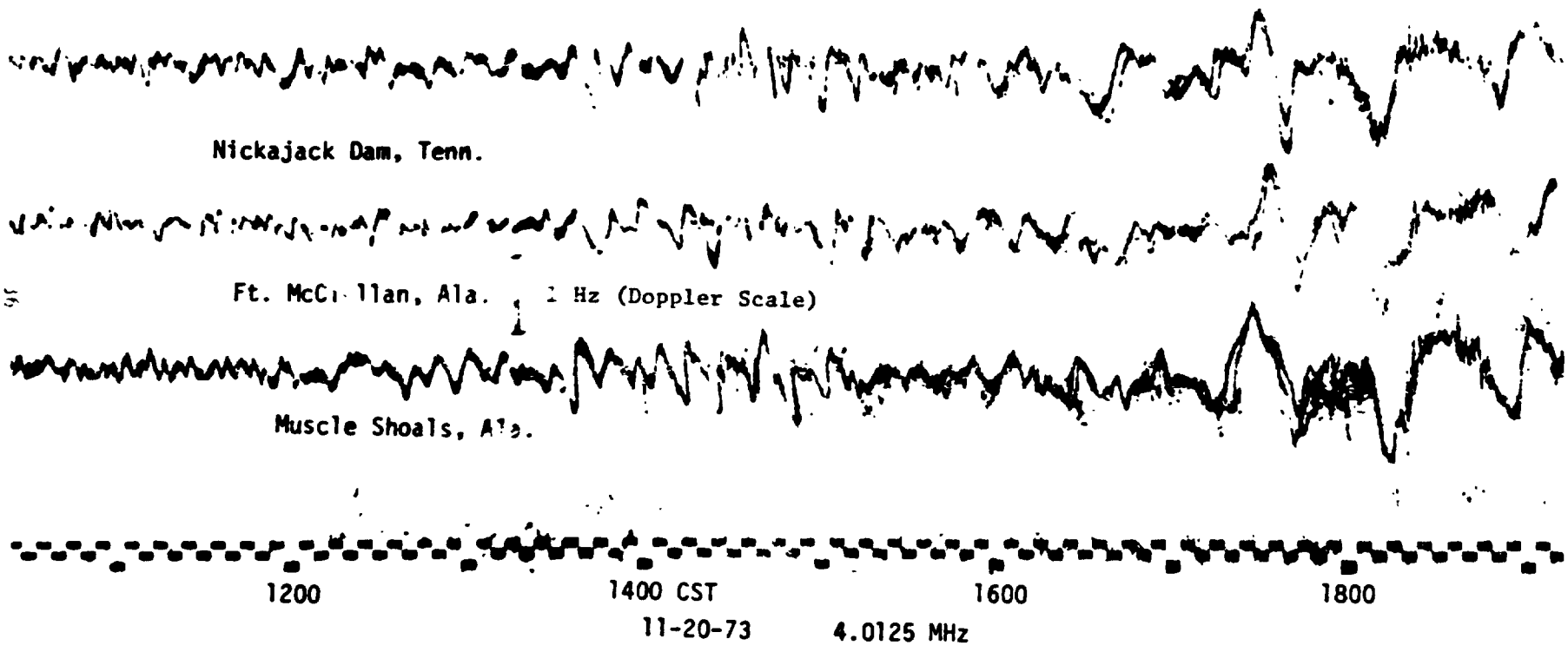

Figure 15. CW Doppler record at the operating frequency of 4.0125 MHz (event on November 20, 1973).

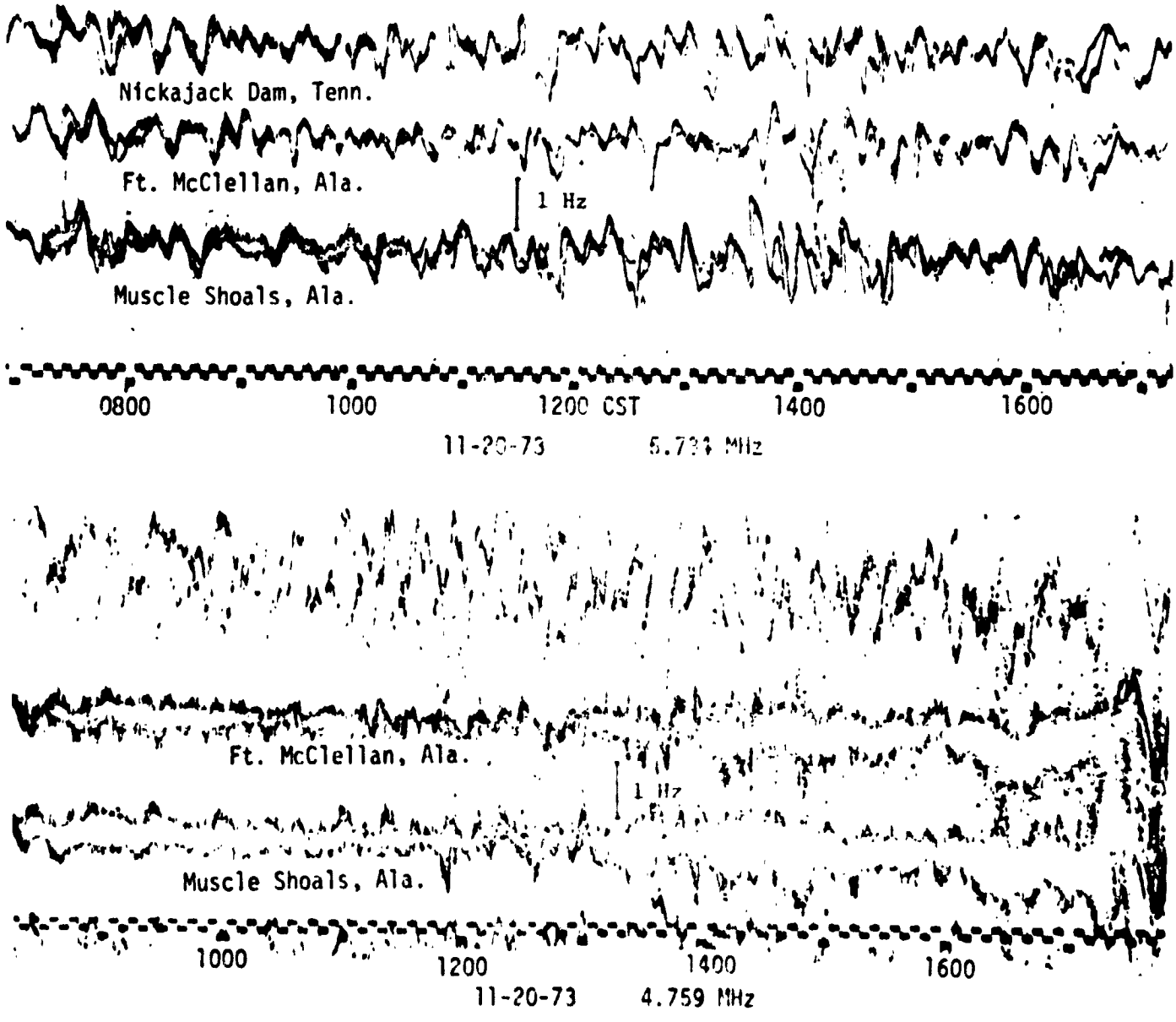

Figure 16. CL Doppler record at the operating frequency of 5.734 and 4.759 MHz (event on November 20, 1973).

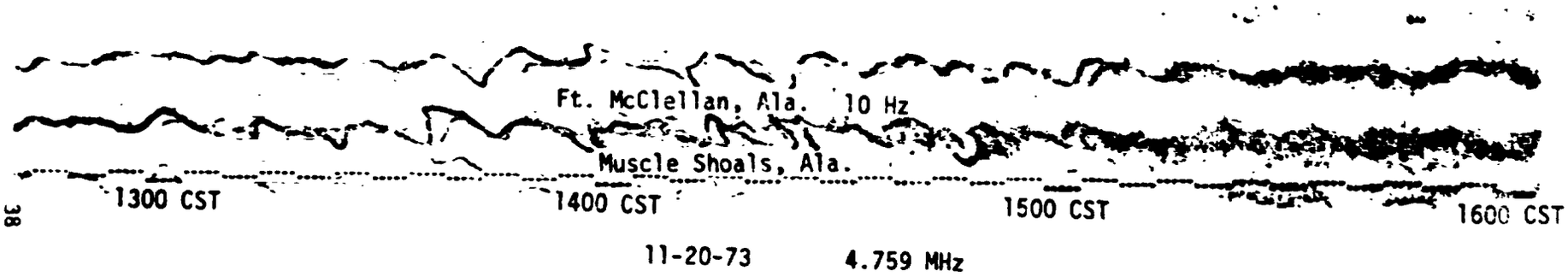

Figure 17. The expansion of time axis of Doppler record on November 20, 1973 at the operating frequency 4.0125 MHz.

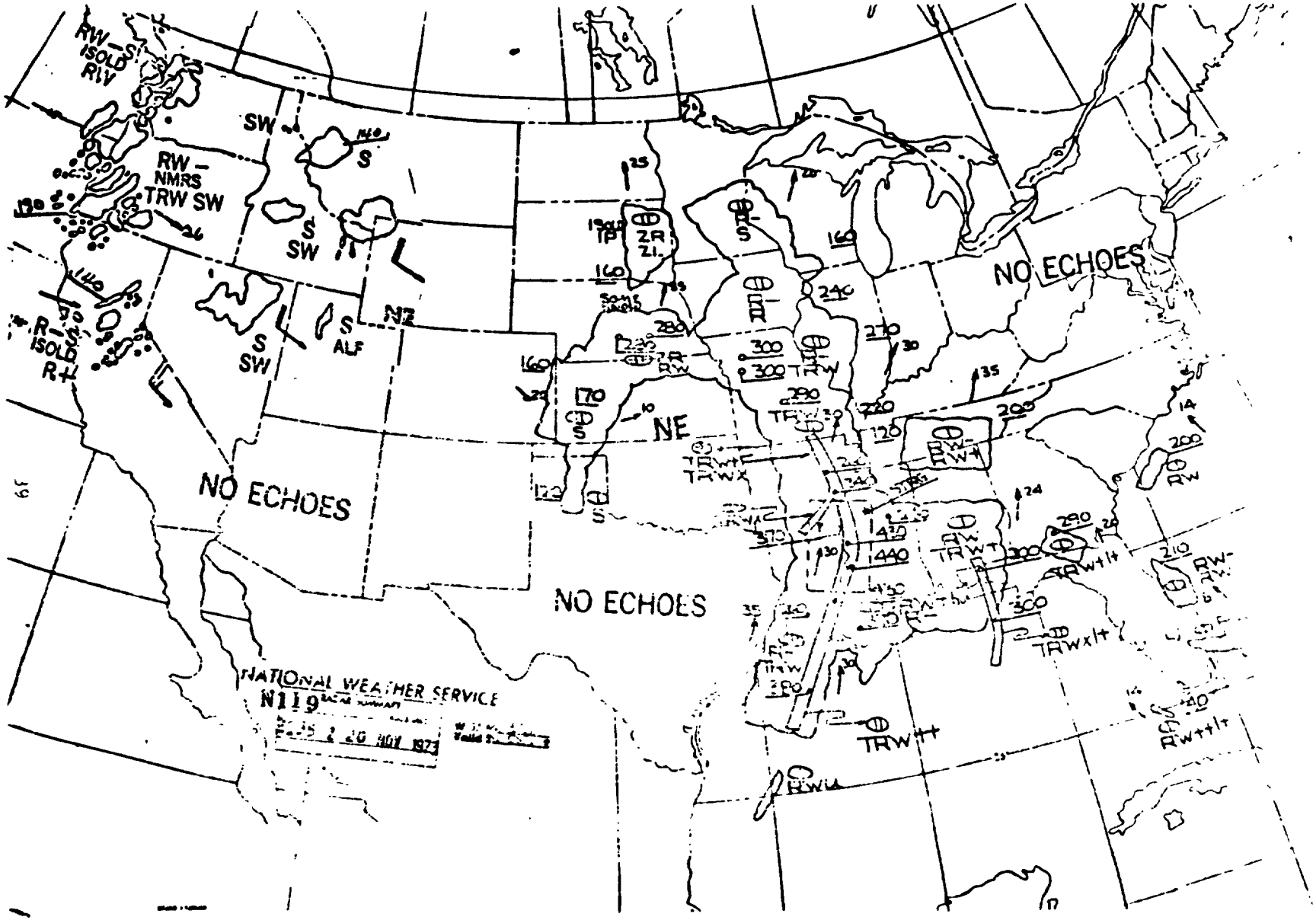

Figure 18. Radar weather summary map at 1535 CST, November 20, 1973.

heights of echo tops are of the order of 40,000 to 50,000 feet (or about 12 to 15 Km). The radar summary charts indicate that the severe weather activity is located southwest of our Doppler array, which is the direction from which the wavelike disturbances seen on Doppler records are propagating.

2. November 27, 1973

Figure 19 shows the Doppler records at the operating frequency of 4.0125 MHz on November 27, 1973 under tornado conditions. This figure clearly shows the wavelike fluctuations beginning about 1100 CST and continuing through the evening hours. The period of the fluctuations obtained from both power spectrum and cross power spectrum analysis are indicated to be on the order of 6 to 8 minutes. The horizontal trace velocities of the disturbances, derived from a cross correlation analysis, are also propagating from the southwest with a magnitude of 600-700 m/sec. The radar weather summary charts for November 27, 1973, are shown in Figure 20. The weather map also clearly shows that the lines radar echoes are from the southwest to the north of the Doppler system. The heights of echo tops are of the order of 40,000 to 50,000 feet (or about 12 to 15 Km). Thus, the radar summary charts indicate that the severe weather activity is located

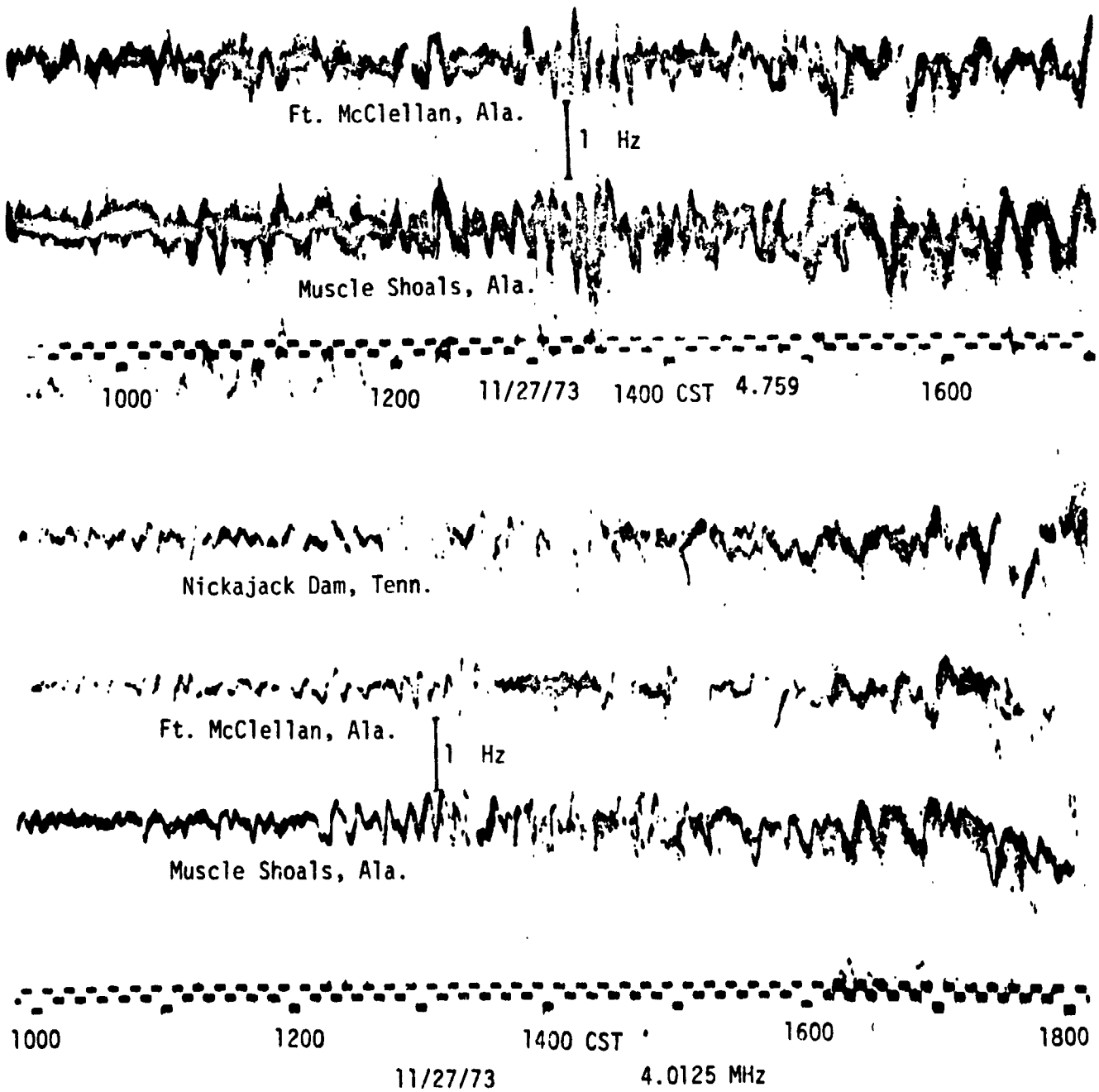

Figure 19. CW Doppler record at the operating frequency of 4.759 and 4.0125 MHz (event on November 27, 1973).

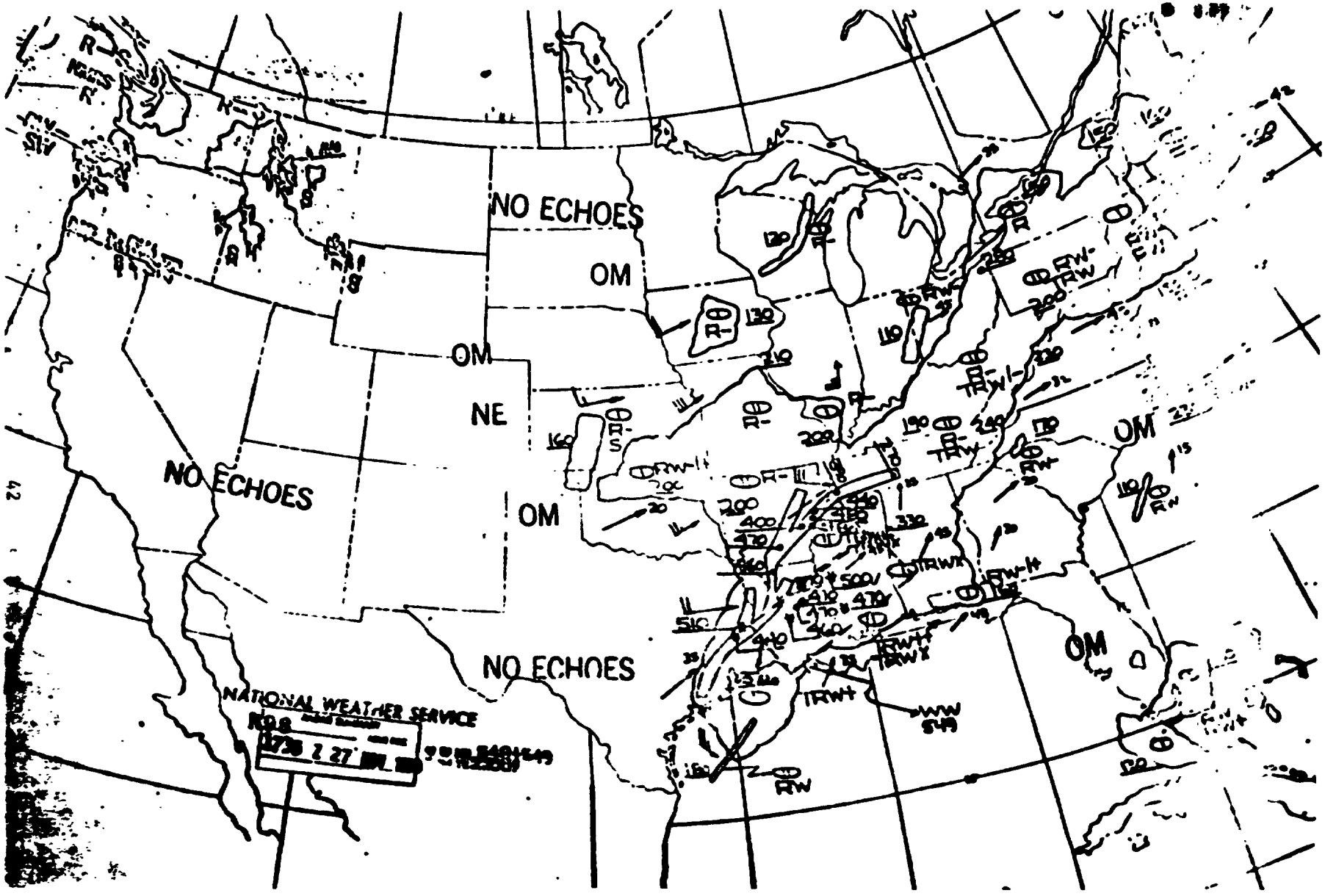

Figure 20. Radar weather summary map at 1135 CST, November 27, 1973.

southwest of our Doppler array, which is the direction from which the wavelike disturbances seen on Doppler records are propagating. The oscillations of Doppler fluctuations in this case persist more than 6 hours.

(3) April 3, 1974

During the extreme tornado outbreak of April 3, 1974, we observed wave-like fluctuations other than the ordinary traveling ionospheric disturbances (TID). Figures 21, 22 and 23 show the CW Doppler records for this day at the operating frequencies of 4.0125, 4.759 and 5.734 MHz, respectively. The observed wave-like fluctuations show several S-shaped Doppler traces or Doppler frequency "fold backs". The periods of these atmospheric waves can be determined by auto-correlating the Doppler records. Figures 24, 25, 26 and 27 show the auto-spectral density of the wave periods observed during different time periods. In Figure 24 three peaks corresponding to waves with periods of 3 min., 6 min., and 11 min. are apparent in the data for the 0700 to 0800 CDT time period. As shown in Figure 4, at 180 Km altitude, the Brunt-Väisälä wave-period is about 10 min. Therefore, waves with 3 min. and 6 min. wave periods are acoustic waves and waves with 11 min. wave periods are gravity waves. The horizontal phase velocity of the disturbances, calculated from a cross-correlation analysis, shows they are propagating in a direction

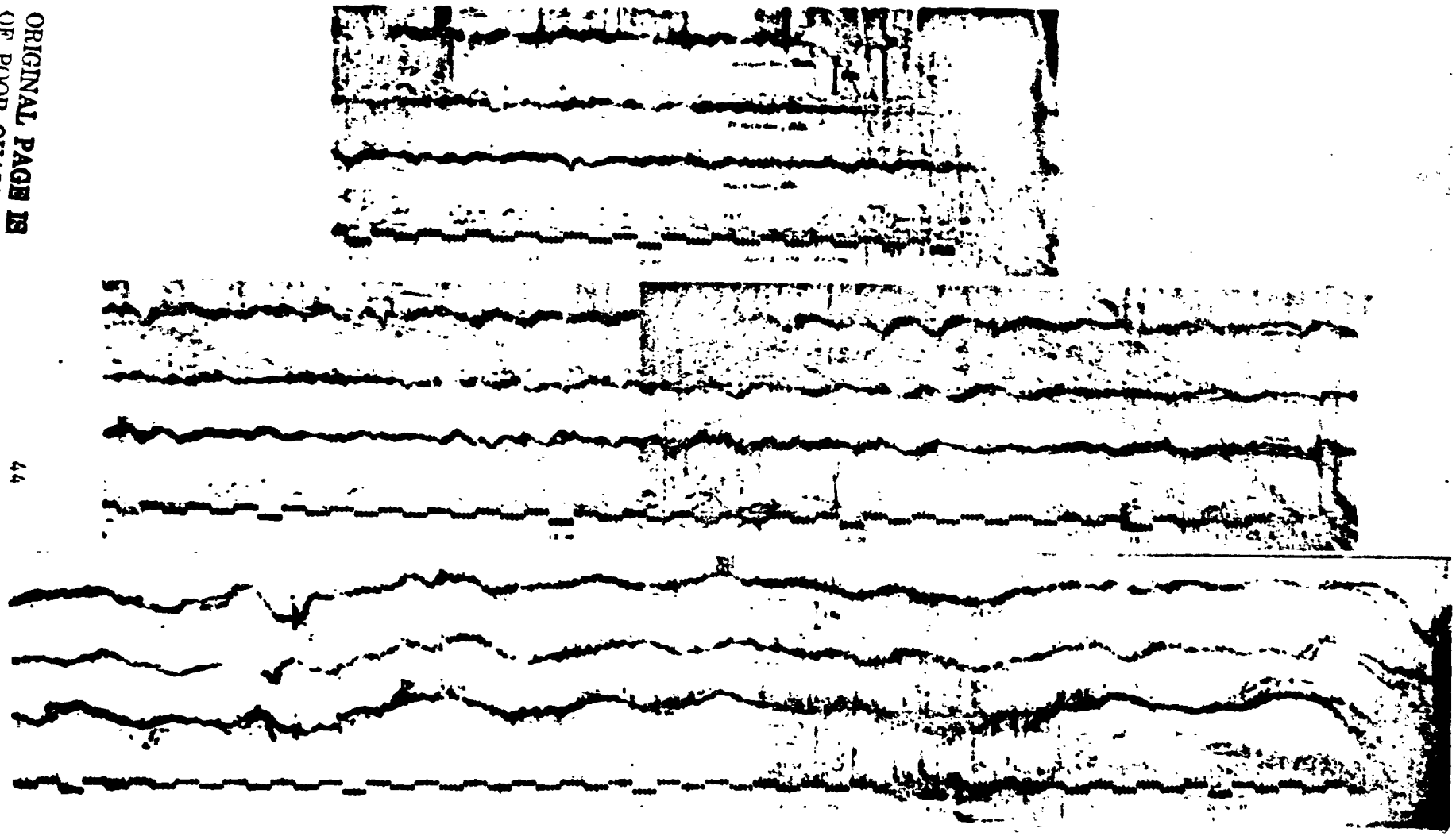

Figure 21. CW Doppler record at the operating frequency 4.0125 MHz (event on April 3, 1974).

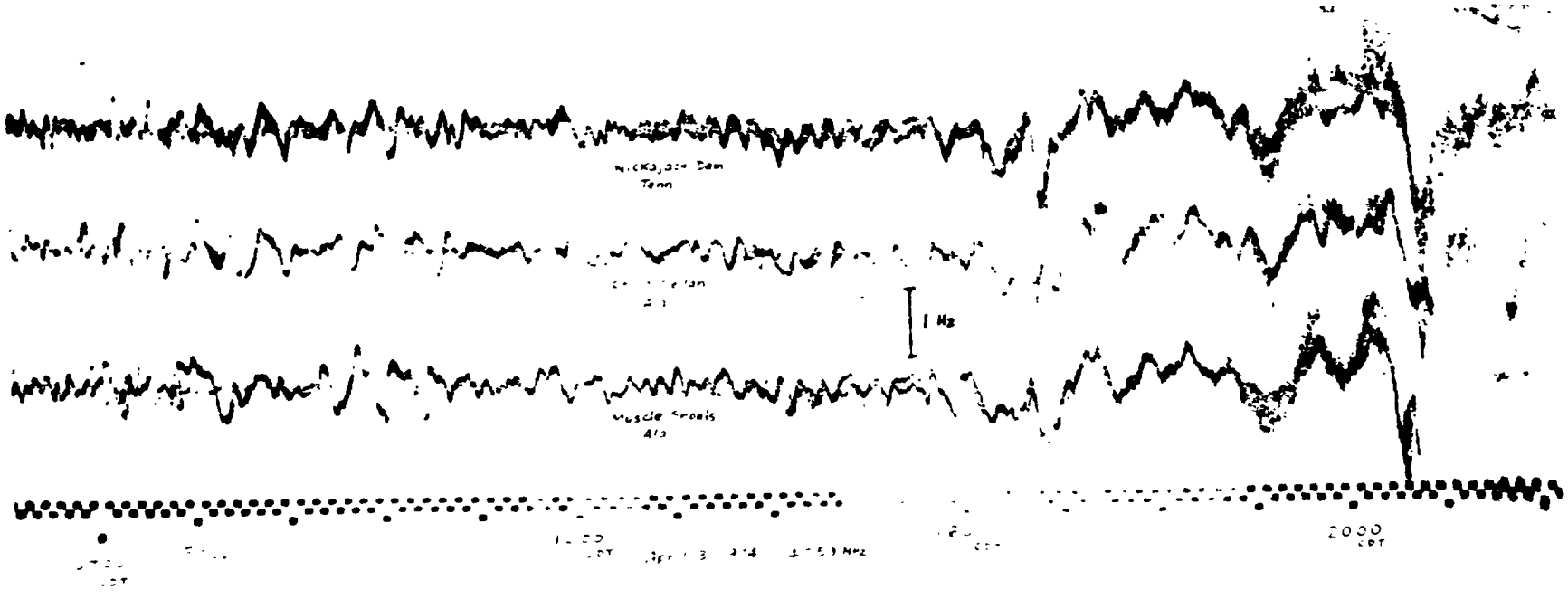

Figure 22. CW Doppler record at the operating frequency 4.759 MHz (event on April 3, 1974).

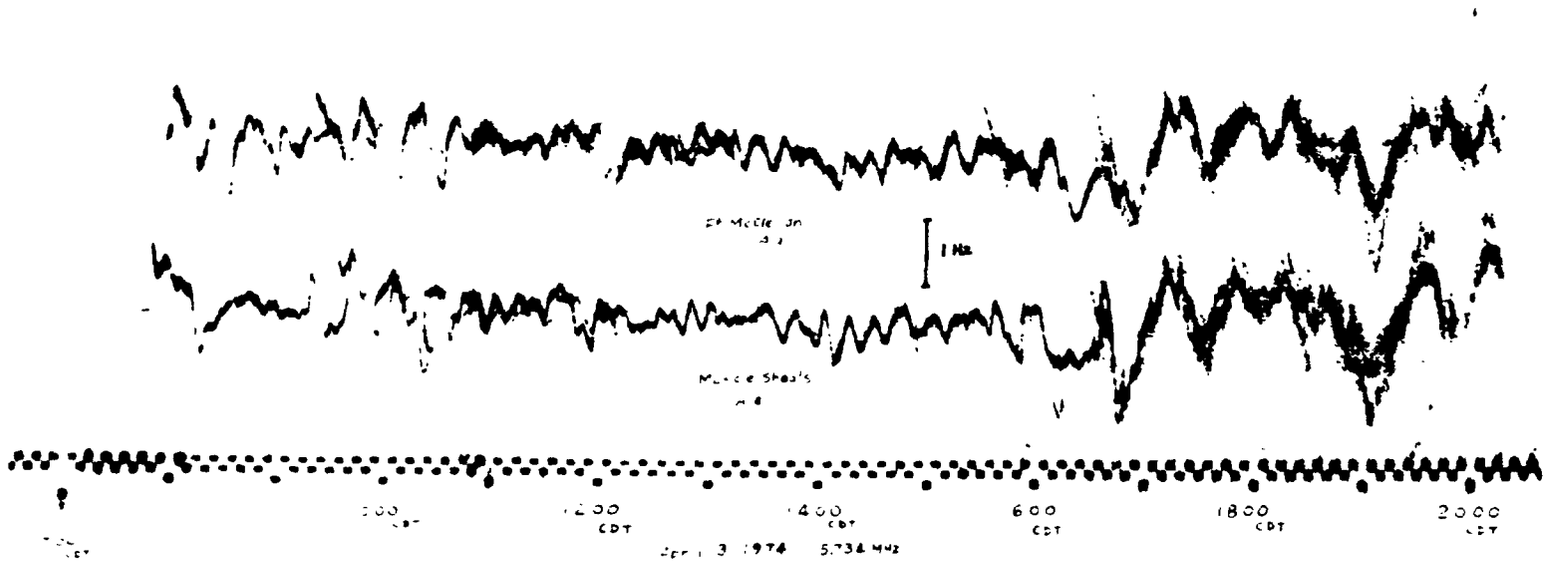

Figure 23. CW Doppler record at the operating frequency 5.734 MHz (event on April 3, 1974).

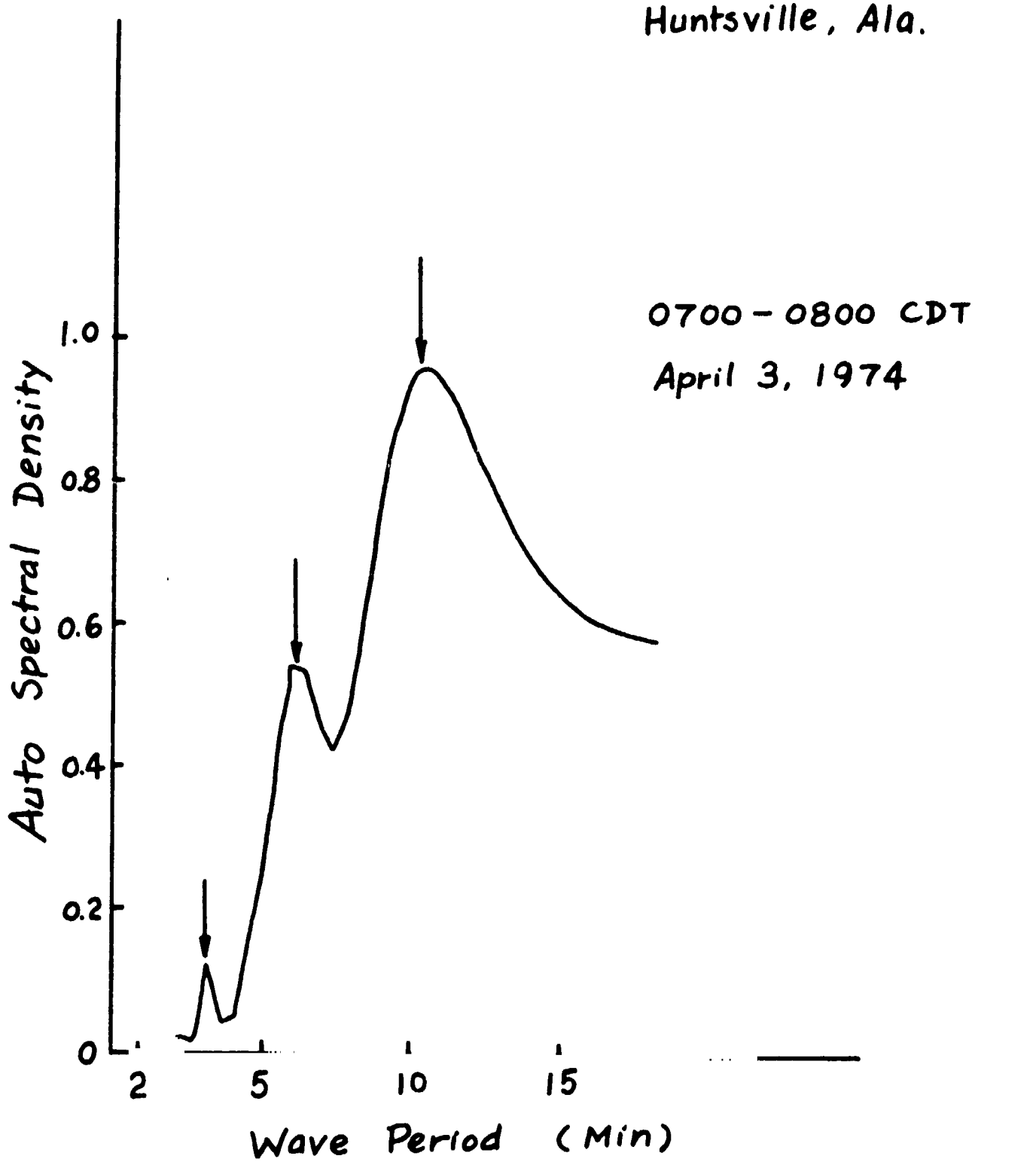

Figure 24. Auto spectrum density of the ionospheric disturbances on April 3, 1974 at 0700-0800 CDT.

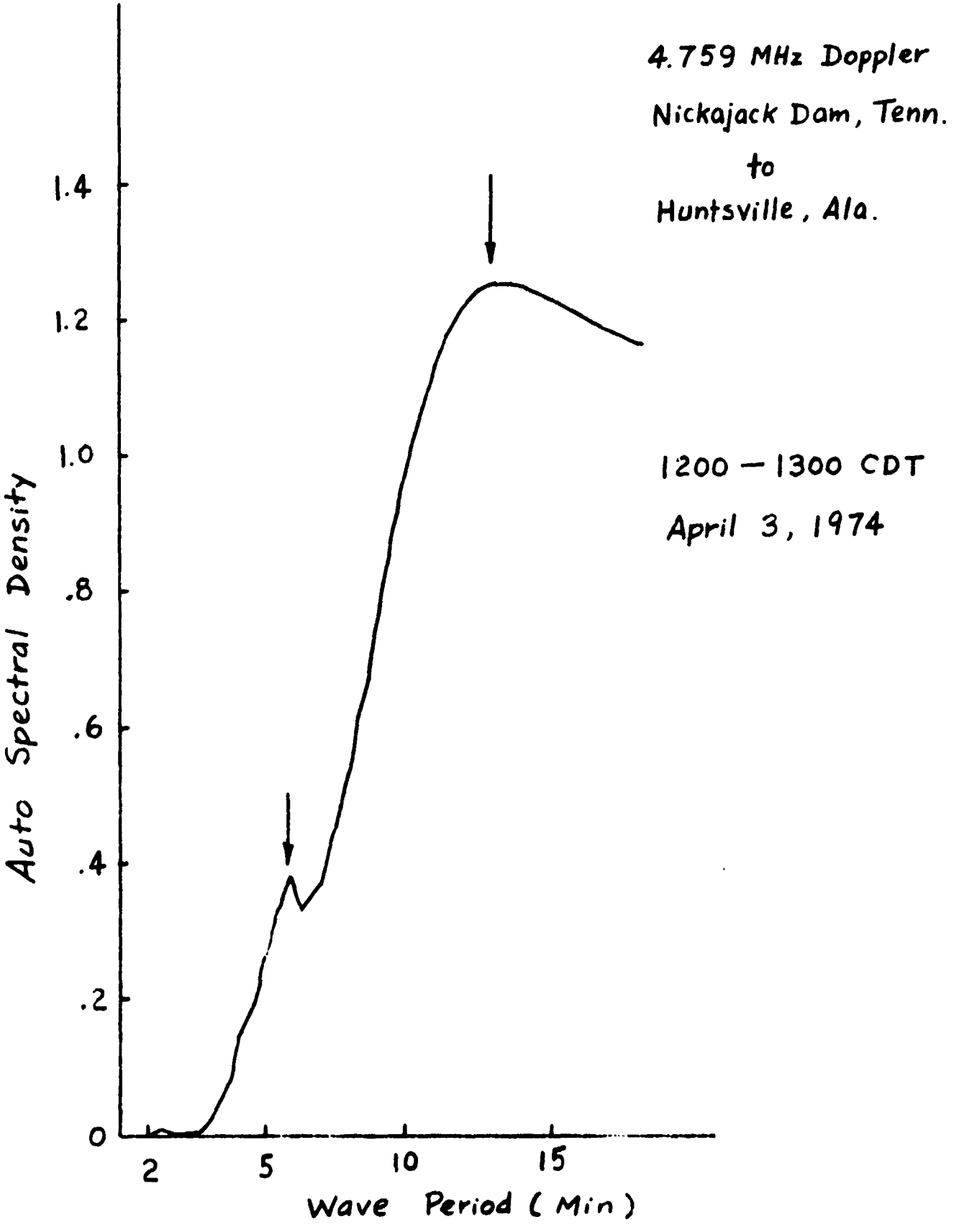

Figure 25. Auto spectrum density of the ionospheric disturbances of April 3, 1974 at 1200-1300 CDT.

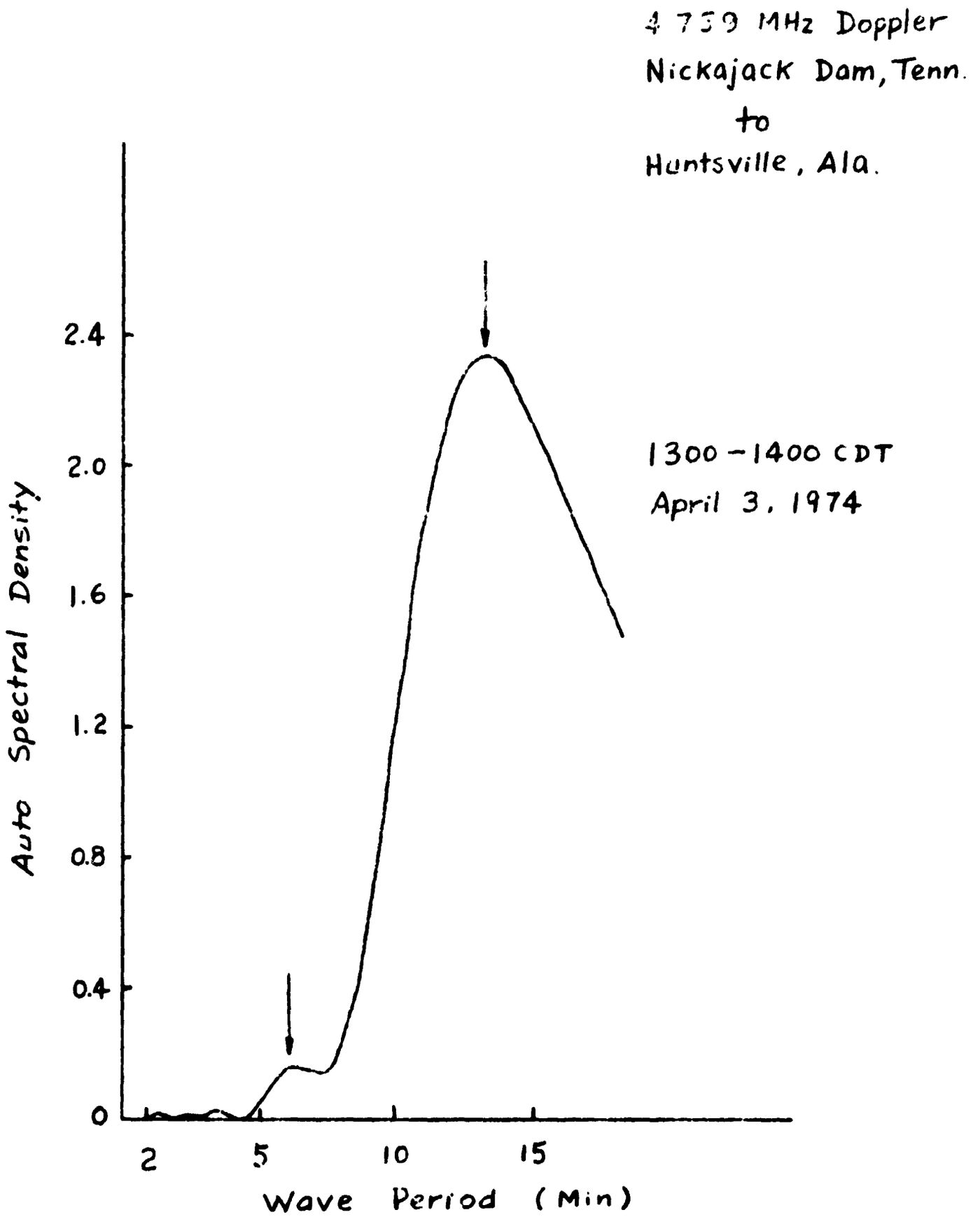

Figure 26. Auto spectrum density of the ionospheric disturbances of April 3, 1974 at 1300-1400 CDT.

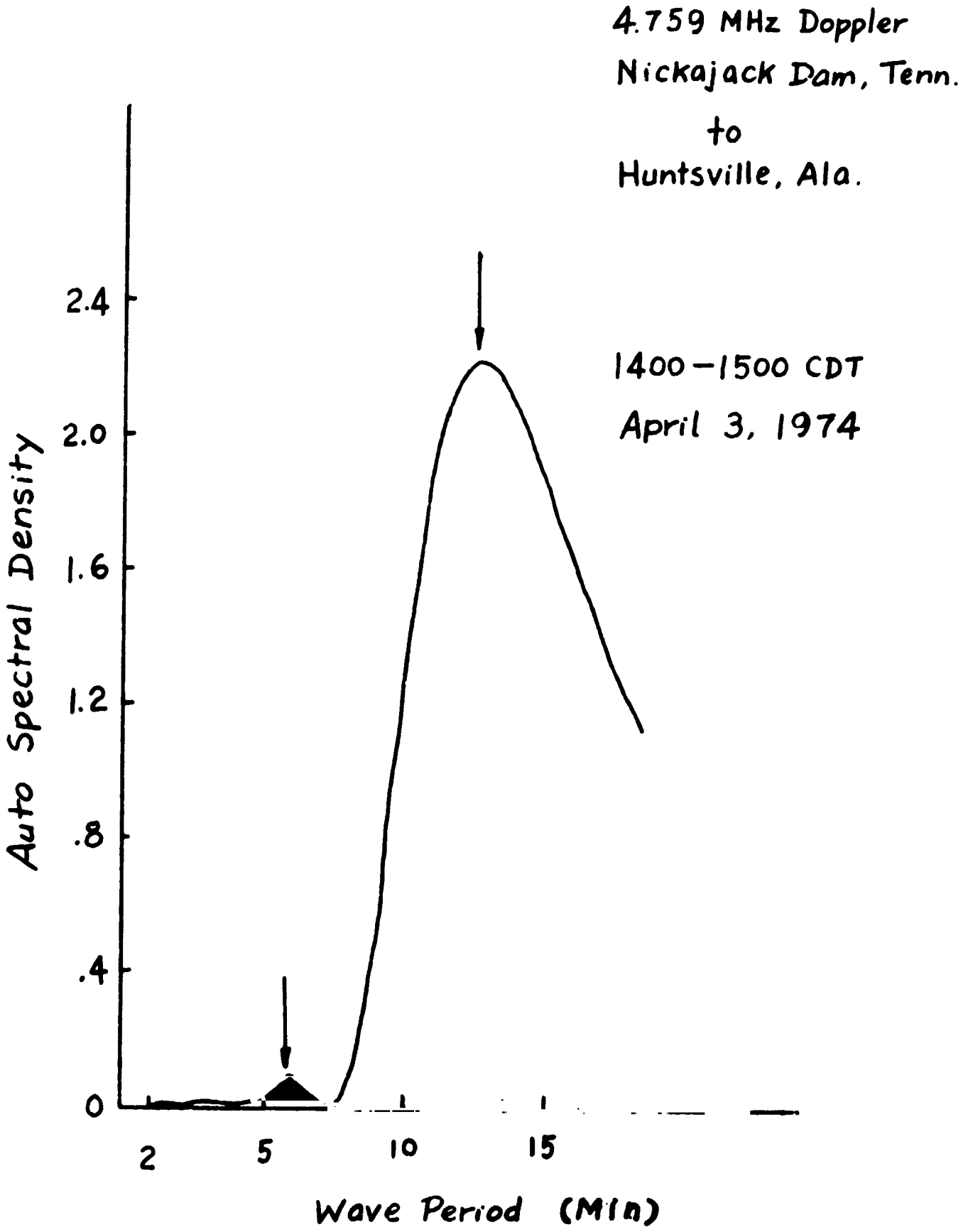

Figure 27. Auto spectrum density of the ionospheric disturbances of April 3, 1974 at 1400-1500 CDT.

103° from geomagnetic north at a speed of 225 m/sec which is a typical phase velocity for gravity waves at F-region ionospheric heights. Gravity waves are predominating over infrasonic waves during 0700 - 0800 CDT time period. Possible sources of the disturbances will be discussed in later sections.

The horizontal phase velocity of the disturbances can be calculated from cross-correlograms. This is because the zero frequency crossings are essentially independent of the amplitude of the change of height of the reflecting surface and they can be used to determine the average period and average time displacement. Figure 28 shows cross-correlograms during the time interval 1400-1500 CDT on 3 April 1975. The average wave-period shown in this cross-correlogram is 13 min. This is in good agreement with the wave-periods during the same time interval obtained from auto-spectral analysis, as shown in Figure 27. The time displacements of the signals between two stations (height peaks from correlograms) are as follows:

$$(\Delta T)_{F\text{-}M} = 650 \text{ sec}$$
$$(\Delta T)_{F\text{-}N} = 330 \text{ sec} \qquad (5\text{-}1)$$
$$(\Delta T)_{N\text{-}M} = 320 \text{ sec}$$

where the subscript F-M denotes the time delay between Ft. McClellan and Muscle Shoals; subscript F-N, time

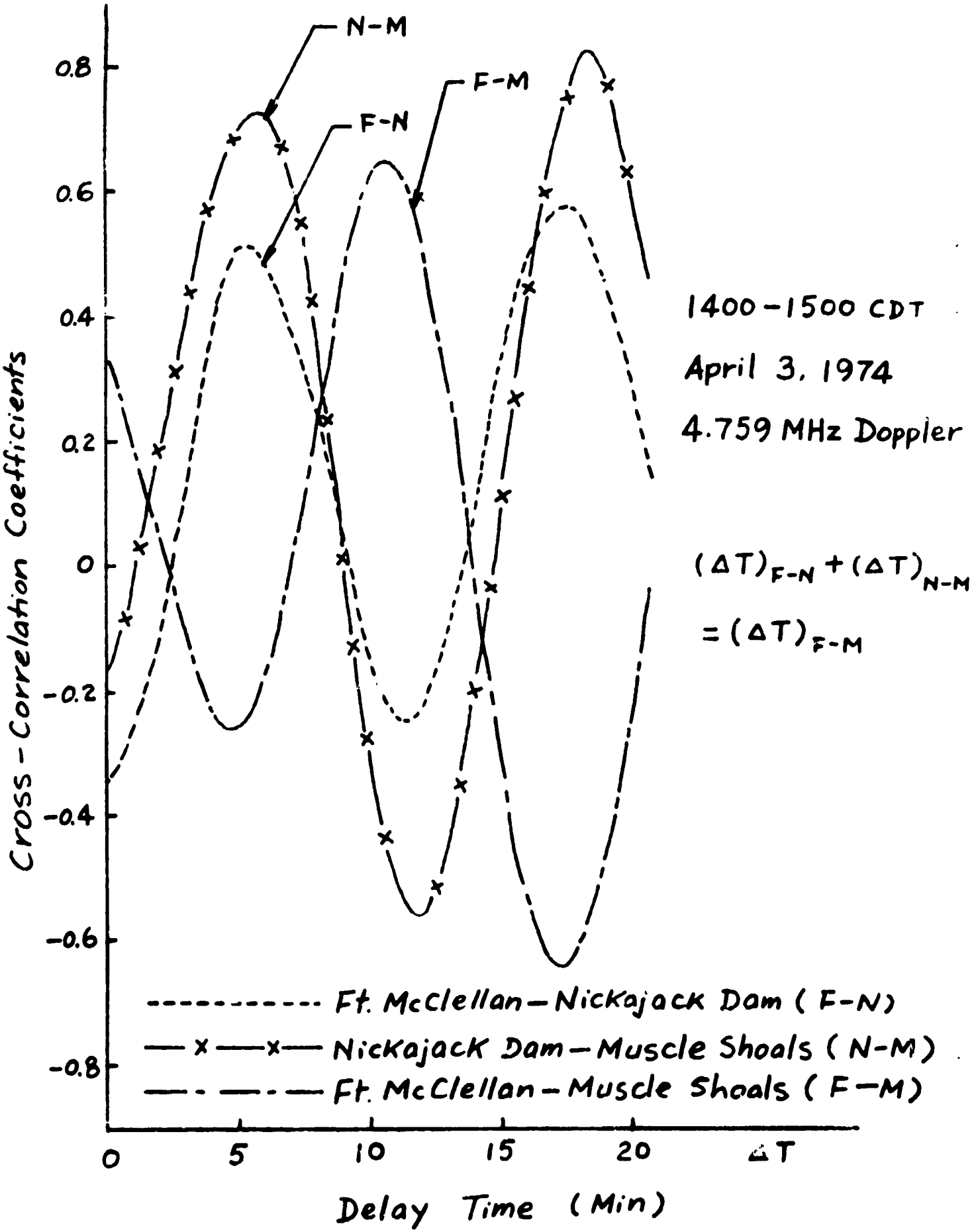

Figure 28. Cross correlograms of the zero crossing from Nickajack Dam (N), Muscle Shoals (M) and Ft. McClellan (F).

delay between Ft. McClellan and Nickajack Dam; and subscript N-M, time delay between Nickajcak Dam and Muscle Shoals. Acceptable combinations of time displacements must satisfy the relationship

$$(\Delta T)_{F-N} + (\Delta T)_{N-M} = (\Delta T)_{F-M} \qquad (5\text{-}2)$$

In our case, it can be shown that the highest peaks of the correlogram, as shown in Equation (5-1), satisfy Equation (5-2). The horizontal phase velocities (both magnitude and direction clockwise from geomagnetic north) during various time intervals on April 3, 1974 are shown in Table 3.

Radar summary charts provided by the National Weather Service, Figures 29, 30, 31 and 32 were used in comparing results calculated from both auto-spectral analysis (Figures 24 to 27) and cross-correlograms (Figure 28 and Table 3) show line echoes and cloud tops from weather radar summaries at different time intervals. During the time interval 0700 to 0800 CDT, Figure 24 and Table 3 show that gravity waves with wave periods of 11 min. and horizontal phase speeds of 225 m/sec propagating from the northwest (towards 103° from north). Figure 29 suggests that the disturbances may have originated in the severe storm cells in the lines of radar echoes with highest

TABLE 3

DOPPLER FLUCTUATIONS OBSERVED DURING SEVERE WEATHER ACTIVITY

DATE	DOPPLER FREQUENCY (MH_Z)	OBSERVED TIME (CDT)	HORIZONTAL TRACE VELOCITY (M/SEC)	DIRECTION (DEGREE FROM MAGNETIC-NORTH)
4-3-1974	4.0125	0700-0800	225	103°
	4.759	1200-1300	101	252
	4.759	1300-1400	217	255
	4.759	1400-1500	160	146

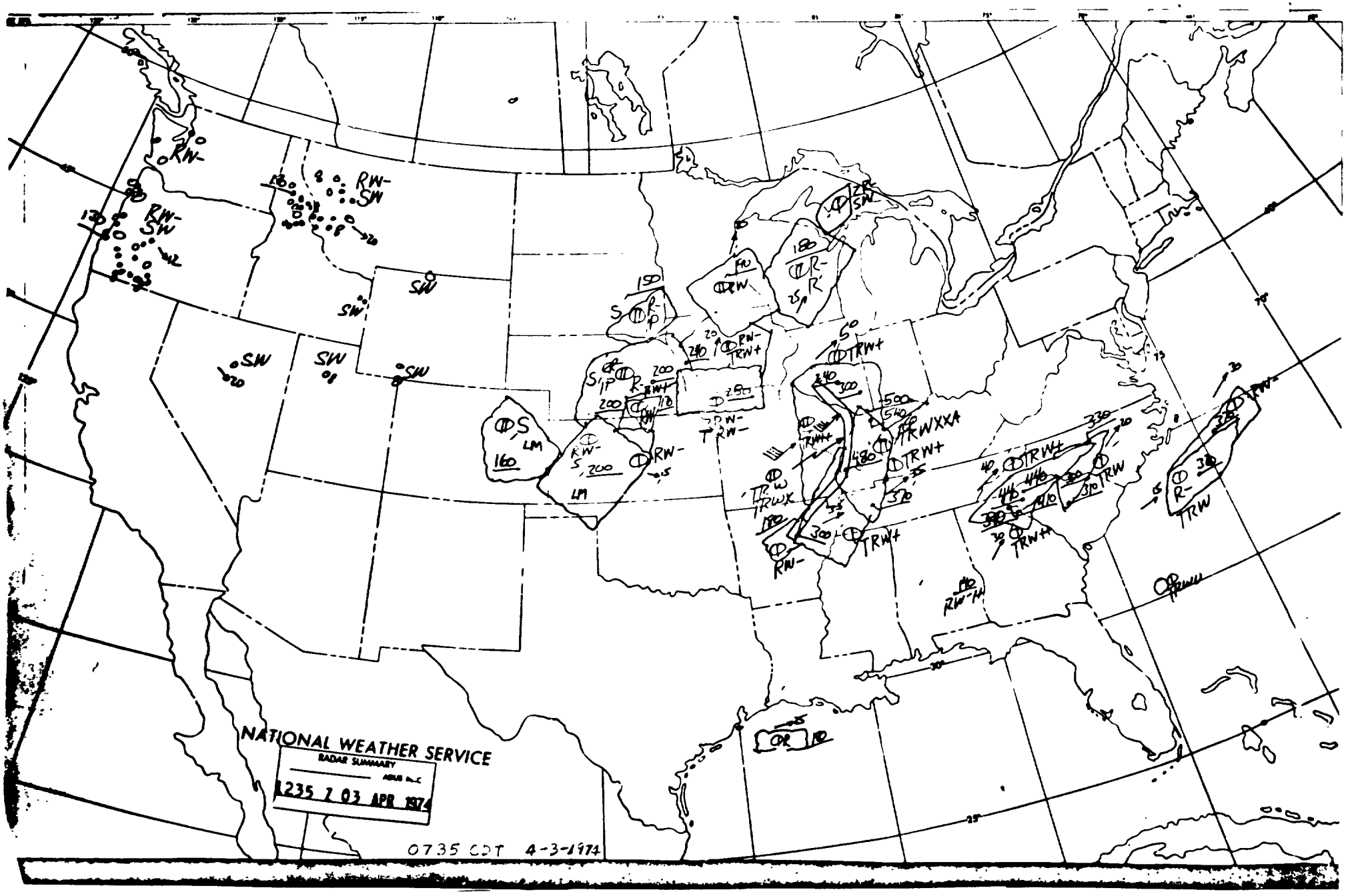

FIGURE 20. RADAR SUMMARY CHART OF APRIL 3, 1974 AT 0735 CDT.

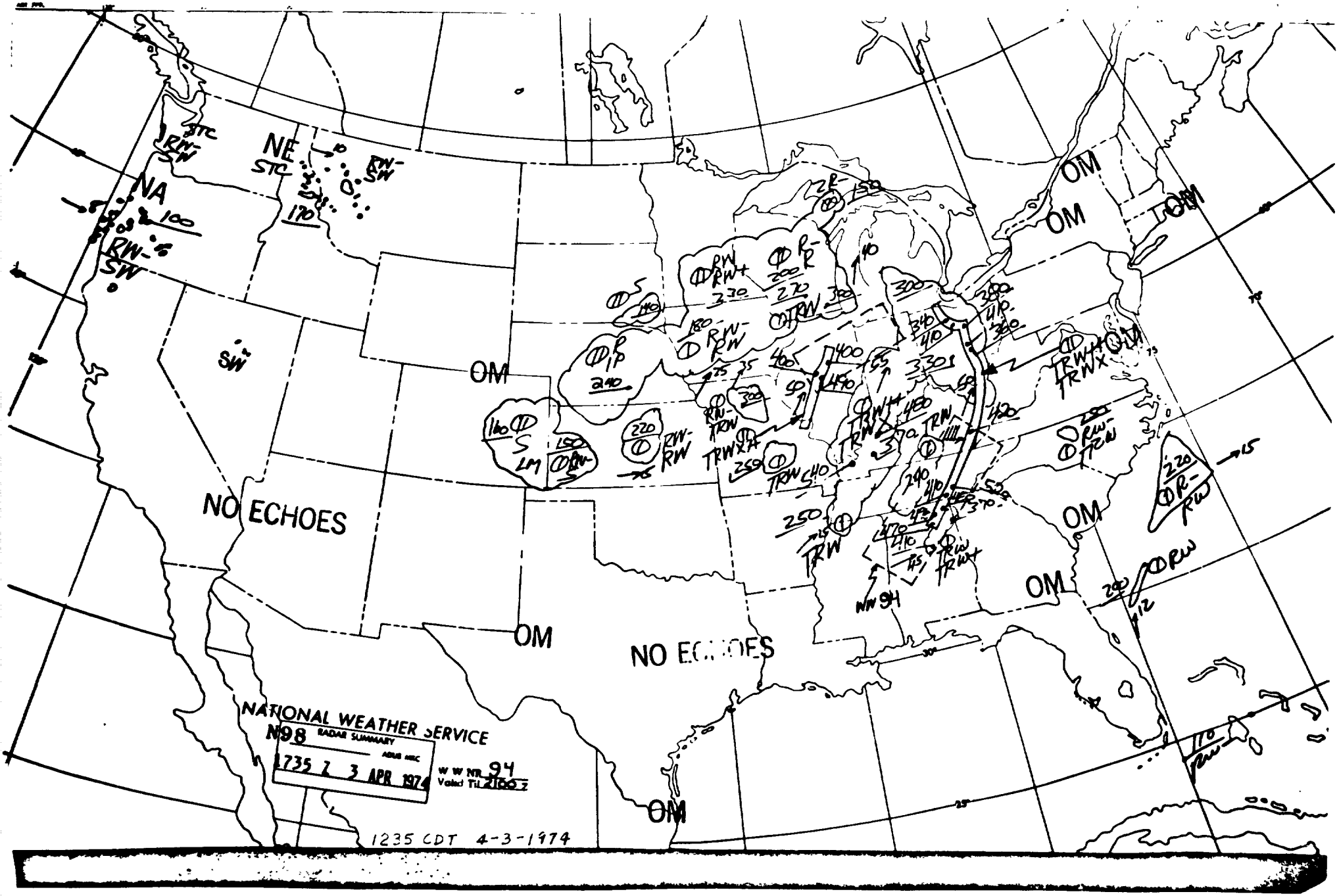

FIGURE 30. RADAR SUMMARY CHART OF APRIL 3, 1974 AT 1235 CDT.

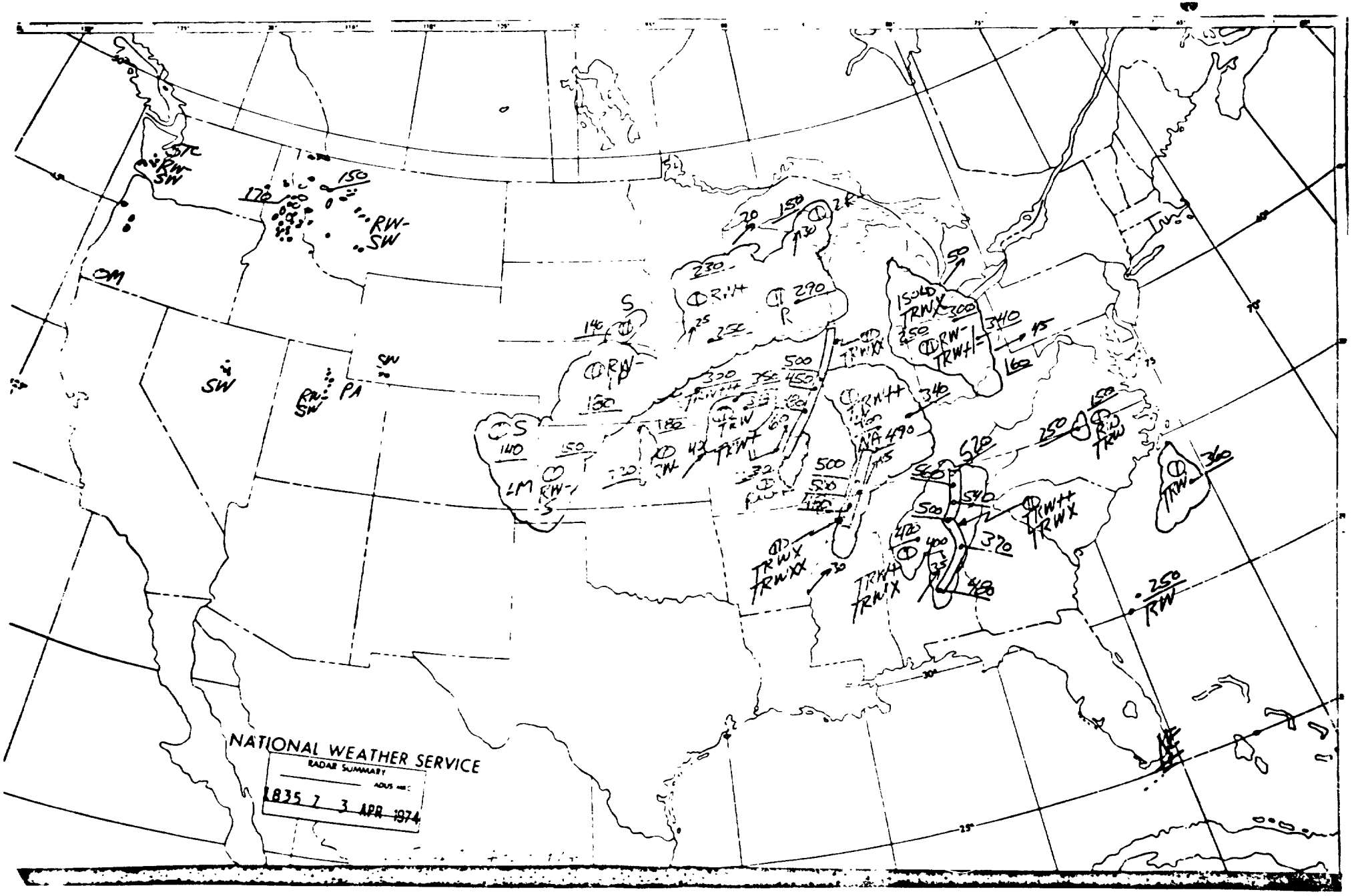

FIGURE 31. RADAR SUMMARY CHART OF APRIL 3, 1974 AT 2335 CDT.

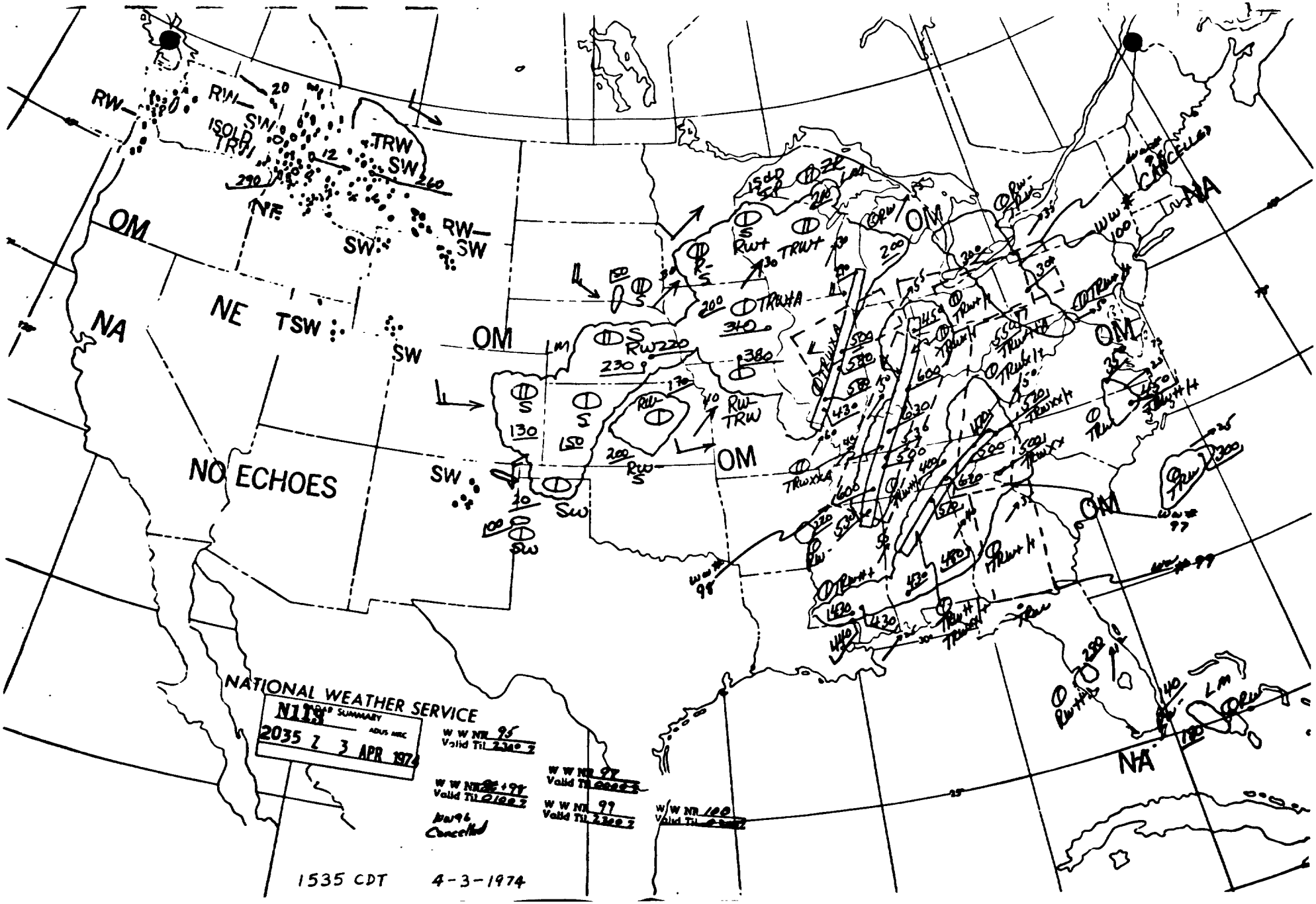

FIGURE 32. RADAR SUMMARY CHART OF APRIL 3, 1974 AT 1535 CDT.

echo tops from 30,000 to 48,000 ft. (or 10 to 15 Km). During the time interval 1200 to 1300 CDT, Figure 25 and Table 3 indicate that gravity waves with wave periods of 12 min. and horizontal phase speeds of 101 m/sec were propagating from the northeast (toward 252° from north). Figure 30 indicates that the source of these disturbances may be in the severe storm cells which are shown in lines of radar echoes with highest echo tops from 47,000 to 50,000 ft. (or 14 to 16 Km). During the time interval 1300 to 1400 CDT, Figure 26 and Table 3 indicate that gravity waves with wave periods of 13 min. and horizontal phase speed of 217 m/sec were propagating from the northeast (toward 225° from north). Figure 31 shows that the source of these disturbances may be in the severe storm cells which are shown in lines of radar echoes with highest echo tops from 37,000 to 56,000 ft. (or 11 to 16 Km). During the time interval 1400 to 1500 CDT, Figure 27 and Table 3 show that gravity waves with wave periods of 12 min. and horizontal phase speeds of 160 m/sec were propagating from the northwest (toward 146° from north).

Again, Figure 32 indicates the source of these disturbances may be in the severe storm cells which are shown in lines of radar echoes with the highest echo tops from 50,000 to 62,000 ft. (or 15 to 19 Km).

VI. DISCUSSIONS AND CONCLUSIONS

Georges (1968; 1973), Baker and Davies (1969), and Davies and Jones (1972) reported observation of ionospheric disturbances during severe storms and suggested that infrasonic waves could be generated by the storm system. During the past two years, the experimental observations accomplished by our group also indicate that infrasonic waves with wave periods of 2 to 8 minutes and with horizontal phase velocity 600-1000 m/sec which is in the range of acoustic velocity at ionospheric height are generated by severe thunderstorm and tornado activity. Furthermore, during the tornado outbreak of April 3, 1974, we observed gravity waves with wave periods of 11 to 13 min. and horizontal phase speeds of 100 to 225 m/sec with several Doppler fold backs in the Doppler records. This result is slightly different from those of the Boulder group; in particular, the gravity waves in this case had wave periods of 11 to 13 min. as compared with the infrasonic waves with wave periods of 3 to 5 min. in the observations by the Boulder Group. However, recent observations made by a Canadian group at London, Ontario, also contained thunderstorm induced gravity waves with wave periods of 12 to 20 min. (Curry and Murry, 1974). Similarily, French and U.K. groups also reported observations of gravity waves with wave periods of the order

of 20 min. in the vicinity of a weather disturbance (Bertin, et.al., 1975).

It is possible that waves with periods of 2 to 8 min. are transformed to waves with periods of 11 to 13 min. by the superimposition of Doppler shifts due to neutral winds by the following relation

$$\omega' = \omega - \underset{\sim}{k} \cdot \underset{\sim}{U} \qquad (6\text{-}1)$$

where ω is the wave frequency observed on the ground; ω', the intrinsic frequency as seen by the observer moving with the wind; $\underset{\sim}{k}$, the wave vector of the disturbances; and $\underset{\sim}{U}$, the wind velocity. However, waves with periods of 2 to 8 min. at ionospheric heights belong to the category of acoustic waves while those with periods of 11 to 13 min. are in the category of gravity waves. This transformation of acoustic waves to gravity waves is possible only when the wave-wave interaction dominates the dynamics of upper atmosphere (Sagdeev and Galeev, 1969). The super-imposition of a Doppler shift due only to neutral winds cannot transform infrasonic waves into gravity waves. This seems to indicate that: (1) severe weather activity is responsible for the generation of both gravity waves and infrasonic waves; and (2) the dynamics of convective motion, wind shear and/or other unknown mechanisms might be responsible for the process of wave-wave inter-action required to transform acoustic waves which were generated by severe weather activity to gravity waves.

The waveforms of the Doppler records shown in Figures 15, 16, 17, 19, 21, 22 and 23 are highly distorted in the S-shaped fasion. This S-shaped record has been explained in terms of a corrugated reflecting surface that moves horizontally with constant speed (Davies and Jones, 1972). We have assumed that the transmitter and receiver both move with speed V while the ionosphere is stationary. If the amplitude of the corrugated surface is A, the mean height of the reflecting surface is H, the path, S, from the transmitter to the reflecting point is given by (Davies and Jones, 1972)

$$S = (H + A \cos \theta)\ (1 + k^2 A^2 \sin^2\theta)^{1/2} \qquad (6\text{-}2)$$

where $\theta = kx$ is the phase of the reflecting point on the corrugated surface, and x is the horizontal spatial axis which the transmitter moves along. The relation between phase, θ, and time, t, is given by

$$\frac{\theta}{k} - kA\ (H + A \cos\theta)\ \sin\theta = Vt \qquad (6\text{-}3)$$

Thus, the instantaneous Doppler shift, Δf, for a carrier frequency, f, is:

$$\frac{\Delta f}{f} = 2kA\,\frac{V}{c}\,\frac{\sin\theta}{(1 + k^2 A^2 \sin^2\theta)^{1/2}}\ x$$

$$x\ [1 - k^2 HA \cos\theta - k^2 A^2 \cos 2\theta] \qquad (6\text{-}4)$$

Davies and Jones (1972) dropped the second and third terms in the square bracket in Equation (6.4). It will be shown later that the second term should have been retained since it is on the order of unity which is essentially the same order as the first term.

For small amplitude waves, $k^2A^2 << 1$, and Equation (6-2) becomes

$$\cos^2\theta + \left(\frac{H}{A}\right)\cos^2\theta - \frac{2}{k^2A^2}\cos\theta + \\ + \frac{2}{k^2H^3}(S - H) = 0 \qquad (6\text{-}5)$$

which is a third order algebraic equation of cos θ. In general, Equation (6-5) has three roots which means that three echoes at different phases can be observed at the same time. However, for a longer wavelength wave, k is shorter. Thus, $2/k^2A^2 >>> 1$, and Equation (6-5) reduces to a first order algebraic equation since $|\cos\theta| \leq 1$. From Equation (6-5) the condition for the existence of multiple-valued echoes is

$$k^2 AH \geq 1 \qquad (6\text{-}6)$$

When this condition exists, the possibility of observing S-shaped Doppler traces is solely dependent on decreasing the wavelength and/or increasing the amplitude of the disturbances.

Equations (6-2), (6-3) and (6-4) have been solved numerically. Figure 33 shows phase path vs. time to reach

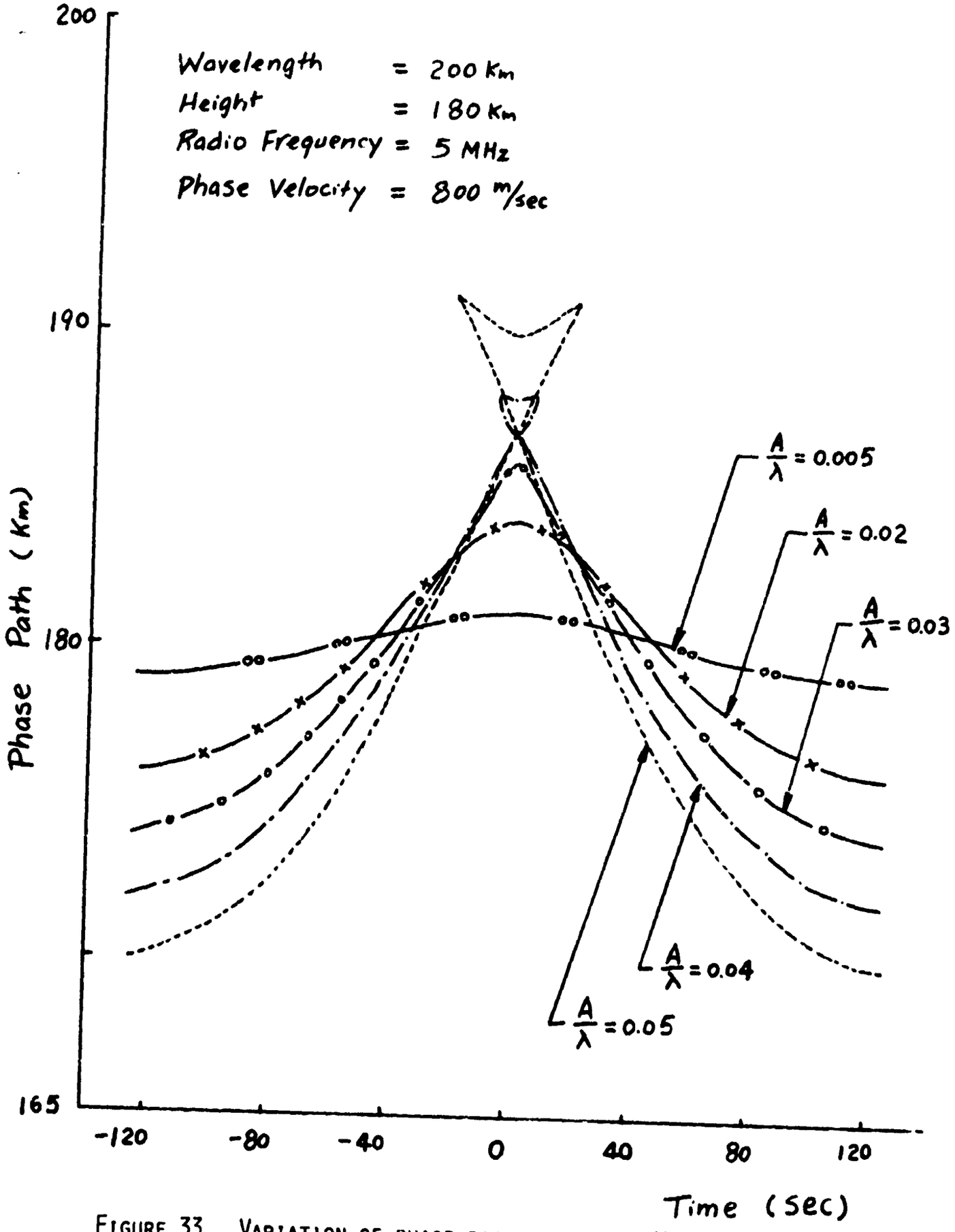

FIGURE 33. VARIATION OF PHASE PATH WITH TIME (A = AMPLITUDE, λ = WAVELENGTH).

the receiver. It is clear that the phase path is sinusoidal when the ratio of the amplitude of the wavelength is less than 0.03. When the ratio of the amplitude to the wavelength is greater than 0.03, it is possible to observe a three-valued phase path. Figure 34 shows the Doppler phase shift, Δf, vs. time to reach the receiver. When the ratio of the amplitude to the wavelength is less than 0.03, the Doppler phase shift is practically quasi-sinusoidal. Doppler fold-backs or S-shaped Doppler traces are formed when the ratio of the amplitude to the wavelength is greater than 0.03 for this case.

In conclusion, the analysis of the Doppler records during the severe weather activity reveals the following results: (1) both infrasonic waves with wave-periods of 2 to 8 min. and with horizontal phase velocity of 600-1000 m/sec, and gravity-waves with wave-periods of 11 to 13 min. and horizontal phase velocity of 100 to 225 m/sec are observed during severe thunderstorm activity and tornado activity; (2) several Doppler fold-backs are observed during the tornado-active day and quasi-sinusoidal wave-profiles are observed during the severe-thunderstorm-active day; (3) the Doppler fold-backs phenomenon is due to radio wave reflection from disturbances where the amplitude to wavelength ratio is high; (4) the eastward wind between the source and the observed fluctuations might be responsible for the change of the wave-period from infrasonic waves to gravity-waves.

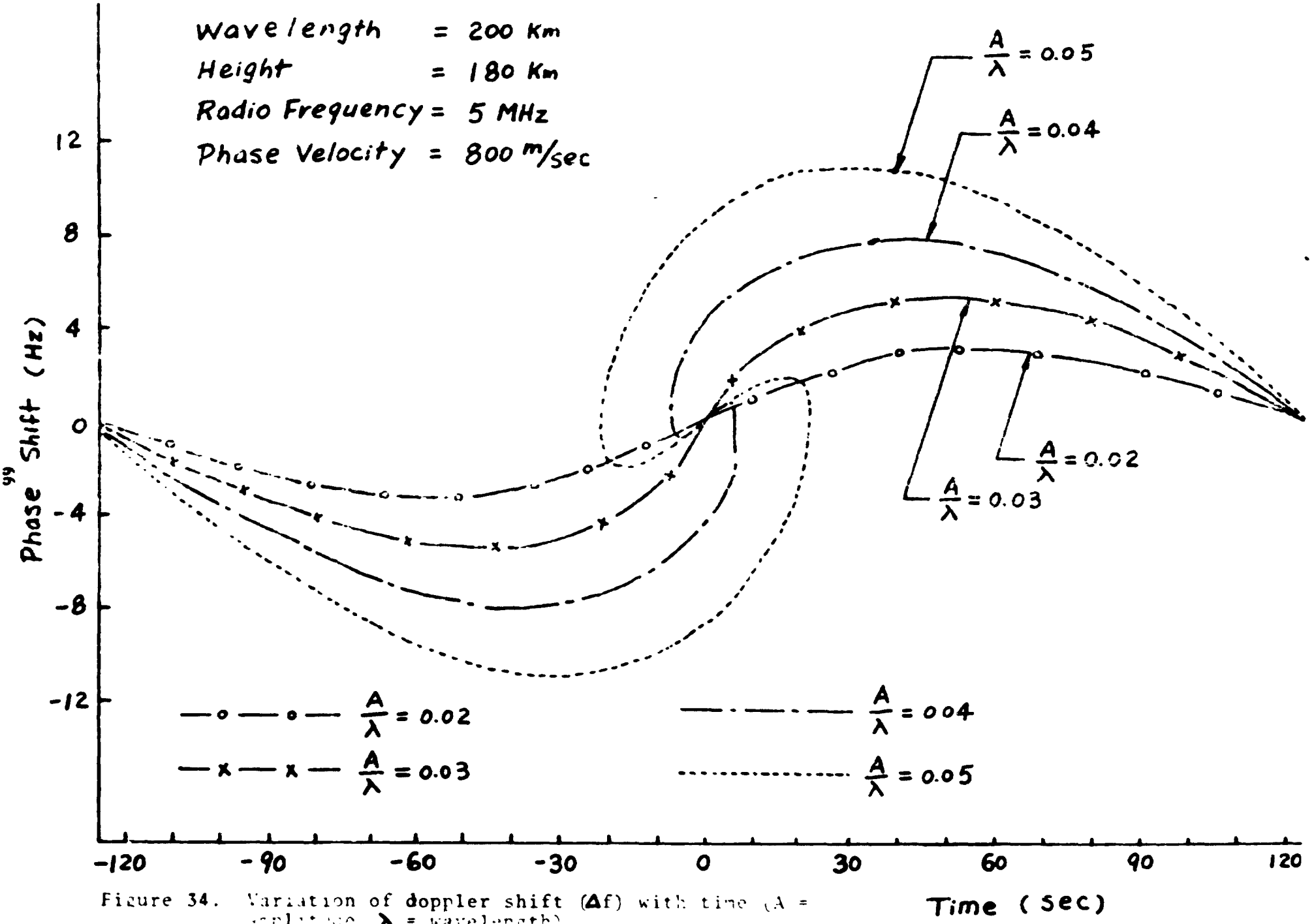

Figure 34. Variation of doppler shift (Δf) with time (A = amplitude, λ = wavelength).

REFERENCES

Baker, D. M. and K. Davies, J. Atmosph. Terr. Phys., 31, 1345, 1969.

Bertin, F., J. Testud and L. Kersley, Planet. Space Sci., 23, 493, 1975.

Brunt, F. A., Quart. J. Roy. Meteor. Soc. 53, 30, 1927.

Curry, M. J. and R. C. Murty, J. Atmosphy. Sci. 31, 1402, 1974.

Davies, K., Proc. IRE 50, 94, 1962.

Davies, K. and D. M. Baker, Radio Sci. 1, 545, 1966.

Davies, K. and J. E. Jones, Space Research XII, Akademic-Verlag, Berlin, 1149, 1972.

Georges, T. M., J. Atmosph. Terr. Phys. 30, 735, 1968.

Georges, T. M., Rev. Geophys. Space Phys. 11, 571, 1973.

Sagdeev, R. Z. and A. A. Galeev, Non-linear Plasma Theory, W. A. Benjamin, Inc., New York, 1969.

APPENDIX

```
MFUN,15 MAIN
FUR AL2C-07/18/75-14:17:30 (,0)

   MAIN PROGRAM

   STORAGE USED: CODE(1) 000742; DATA(0) 010667; BLANK COMMON(2) 000000


   EXTERNAL REFERENCES (BLOCK, NAME)

    0003    POWDEN
    0004    PRTPLT
    0005    NINTR$
    0006    NRDU$
    0007    NI03$
    0010    NI01$
    0011    NI02$
    0012    NWDU$
    0013    NSTOP$


   STORAGE ASSIGNMENT  (BLOCK, TYPE, RELATIVE LOCATION, NAME)

    0000    010456 1F       0000    010542 10F      0000    010556 11F      0000    010571 12F      0001    000016 120G
    0001    000023 124G     0000    010602 13F      0000    010620 14F      0001    000046 140G     0001    000046 142G
    0000    010522 15F      0001    000104 152G     0001    000114 157G     0000    010503 16F      0001    000125 165G
    0001    000140 176G     0001    000002 20L      0001    000152 204G     0001    000202 240G     0001    000212 225G
    0001    000225 236G     0001    000234 243G     0001    000262 256G     0001    000272 263G     0001    000305 273G
    0000    010460 3F       0001    000314 300G     0001    000342 312G     0001    000352 317G     0001    000365 327G
    0000    010635 33F      0001    000374 334G     0001    000412 343G     0001    000422 350G     0001    000435 360G
    0001    000444 365G     0001    000472 377G     0000    010461 4F       0001    000502 404G     0001    000515 414G
    0001    000524 421G     0001    000552 433G     0001    000562 440G     0001    000575 450G     0001    000604 455G
    0001    000635 470G     0000    010465 5F       0000    010463 50F      0001    000651 500G     0001    000660 505G
    0001    000670 514G     0001    000707 525G     0001    000712 530G     0000    010505 6F       0000    010510 7F
    0000    010524 8F       0000    010527 9F       0000 R  002247 A        0000 R  004053 COH      0000 R  006373 COR
    0000 R  005657 DEVD     0000 R  010204 ENGI     0000 R  000443 F        0000 R  004755 G        0000 I  010200 I
    0000 I  000063 IN       0000 I  010177 IT       0000 I  010201 J        0000 I  010205 K        0000 I  010202 L
    0000 I  010203 LI       0000 R  003151 PH       0000 R  001345 W        0000 R  006145 S        0000 R  007751 SL
    0000 R  006047 TITLE    0000 R  010206 X        0000 R  007275 XBR      0000 R  007523 XBRL     0000 R  010332 XS
    0000 R  000000 Y        0000 R  010404 YS       0000 R  010260 Z


00101      1*          PARAMETER NQ=40                                                          000000
00103      2*          PARAMETER IP=42                                                          000002
00104      3*          PARAMETER N=97                                                           000002
00105      4*          PARAMETER NSERS=3                                                        000002
00106      5*          PARAMETER M=50                                                           000002
00107      6*          DIMENSION Y(N,NSERS),F(NSERS,NSERS,M),Q(NSERS,NSERS,M),A(NSERS,          000002
00107      7*         *NSERS,M),PH(NSERS,NSERS,M)                                               000002
00110      8*          DIMENSION COH(NSERS,NSERS,M),G(NSERS,NSERS,M),DEVD(NSERS,NQ),            000002
00110      9*         *TITLE(12),IN(M),S(NSERS,M)                                               000002
00111     10*          DIMENSION COR(NSERS,NSERS,M),XBR(NSERS,M),XBRL(NSERS,M),SL(NSERS,        000002
00111     11*         *M)                                                                       000002
00112     12*        20 READ(5,1)TITLE,IT                                                       000002
00116     13*         1 FORMAT(12A6/I5)                                                         000016
```

```
00117    14.          DO 25 I=1,NSERS                                                    000016
00122    15.       25 READ(5,3)(Y(J,I),J=1,N)                                            000016
00131    16.        3 FORMAT(     )                                                      000027
00132    17.          WRITE(6,4)TITLE                                                    000027
00135    18.        4 FORMAT(1H1,12A6)                                                   000037
00136    19.          WRITE(6,50)((Y(J,I),J=1,N),I=1,NSERS)                              000037
00147    20.       50 FORMAT(12F6.2)                                                     000051
00150    21.          CALL POWDEN(Y,N,NSERS,M,NW,IT,COR,F,Q,A,PH,COH,G,DEVD,N,NSERS,M,   000051
00150    22.         * NW,XBR,XBRL,S,SL)                                                000104
00151    23.          DO 26 J=1,NSERS                                                    000104
00154    24.       26 IN(J)= J                                                           000114
00156    25.          DO 27 I=1,NSERS                                                    000114
00161    26.          WRITE(6,5) I,I,(IN(J),J=1,NSERS)                                   000130
00171    27.        5 FORMAT(38HCROSS CORRELATIONS RELATIVE TO SERIES I4/                000130
00171    28.         *10X,4HCOR(I2, 5H,J,L)/10H SERIES    6I8)                         000130
00172    29.          WRITE(6,16)                                                        000140
00174    30.       16 FORMAT(4H LAG)                                                     000140
00175    31.          DO 27 L=1,M                                                        000140
00200    32.          L1=L-1                                                             000143
00201    33.       27 WRITE(6,6)L1,(COR(I,J,L),J=1,NSERS)                                000164
00212    34.        6 FORMAT(1H I3,6A,6F8.4)                                             000164
00213    35.          WRITE(6,4) TITLE                                                   000174
00216    36.          ENW1=NW-1                                                          000202
00217    37.          DO 35 I=1,NSERS                                                    000202
00222    38.          WRITE(6,7)I,(IN(K),K=1,NSERS)                                      000215
00231    39.        7 FORMAT(40HCOSPECTRAL DENSITIES RELATIVE TO SERIES14/7H SERIES618)  000215
00232    40.          WRITE(6,15)                                                        000225
00234    41.       15 FORMAT(7H PERIOD)                                                  000225
00235    42.          DO 35 K=1,NW                                                       000225
00240    43.       35 WRITE(6,8)K,(F(I,J,K),J=1,NSERS)                                   000246
00251    44.        8 FORMAT(1H I5,5X,6F8.5)                                             000246
00252    45.          WRITE(6,4)TITLE                                                    000262
00255    46.          DO 36 I=1,NSERS                                                    000262
00260    47.          WRITE(6,9)I,(IN(K),K=1,NSERS)                                      000275
00267    48.        9 FORMAT(40HQUADRATURE DENSITIES RELATIVE TO SERIES I4/               000275
00267    49.         *10H SERIES    6I8)                                               000275
00270    50.          WRITE(6,15)                                                        000305
00272    51.          DO 36 K=1,NW                                                       000305
00275    52.       36 WRITE(6,8)K,(Q(I,J,K),J=1,NSERS)                                   000326
00306    53.          WRITE(6,4)TITLE                                                    000342
00311    54.          DO 37 I=1,NSERS                                                    000342
00314    55.          WRITE(6,10     ,N(K),K=1,NSERS)                                    000355
00323    56.       10 FORMAT(45      35 SPECTRAL AMPLITUDES RELATIVE TO SERIES I4/       000355
00323    57.         *10H SERIES     6I8)                                               000355
00324    58.          WRITE(6,15)                                                        000365
00326    59.          DO 37 K=1,NW                                                       000365
00331    60.       37 WRITE(6,8)K,(A(I,J,K),J=1,NSERS)                                   000412
00342    61.          DO 38 I=1,NSERS                                                    000412
00345    62.          WRITE(6,11)I,(IN(K),K=1,NSERS)                                     000425
00354    63.       11 FORMAT(41HCROSS SPECTRAL PHASES RELATIVE TO SERIES I4/             000425
00354    64.         *10H SERIES    6I8)                                               000425
00355    65.          WRITE(6,15)                                                        000435
00357    66.          DO 38 K=1,NW                                                       000435
00362    67.       38 WRITE(6,8)K,(PH(I,J,K),J=1,NSERS)                                  000456
00373    68.          WRITE(6,4)TITLE                                                    000472
00376    69.          DO 39 I=1,NSERS                                                    000472
00401    70.          WRITE(6,12)I,(IN(K),K=1,NSERS)                                     0004??
```

```
00410     71.       12 FORMAT(46HOCROSS SPECTRAL COHERENCES RELATIVE TO SERIES     618)                000505
00411     72.          WRITE(6,15)                                                                    000505
00413     73.          DO 39 K=1,NQ                                                                   000515
00416     74.       39 WRITE(6,8)K,(COH(I,J,K),J=1,NSERS)                                             000515
00427     75.          WRITE(6,4)TITLE                                                                000536
00432     76.          DO 40 I=1,NSERS                                                                000552
00435     77.          WRITE(6,13)I,(IN(K),K=1,NSERS)                                                 000552
00444     78.       13 FORMAT(31HOCROSS SPECTRAL GAINS OF SERIES I3,21H RELATIVE TO SERIE             000565
00444     79.         1S J 10H SERIES    618)                                                         000565
00445     80.          WRITE(6,15)                                                                    000565
00447     81.          DO 40 K=1,NQ                                                                   000575
00452     82.       40 WRITE(6,8)K,(G(I,J,K),J=1,NSERS)                                               000575
00463     83.          WRITE(6,4)TITLE                                                                000616
00466     84.          WRITE(6,14)(IN(K),K=1,NSERS)                                                   000626
00474     85.       14 FORMAT(51HOSTANDARD DEVIATION OF THE AUTO SPECTRAL DENSITIES /                  000640
00474     86.         11OH SERIES    618)                                                            000640
00475     87.          WRITE(6,15)                                                                    000640
00477     88.          DO 41 K=1,NQ                                                                   000651
00502     89.       41 WRITE(6,8)K,(DEVD(I,K),I=1,NSERS)                                              000651
00502     90.     C       PLOT  CURVE                                                                 000651
00512     91.          DIMENSION X(IP),Z(IP),XS(IP),YS(IP)                                            000670
00513     92.          DO 2 I=1,NQ                                                                    000670
00516     93.        2 X(I+1)=FLOAT(I)                                                                000670
00520     94.          X(IP)=80.0                                                                     000675
00521     95.          Z(IP)=2.0                                                                      000677
00522     96.          X(1)=0.0                                                                       000701
00523     97.          Z(1)=0.0                                                                       000702
00524     98.          DO 34 I=1,NSERS                                                                000712
00527     99.          DO 32 J=1,NQ                                                                   000712
00532    100.       32 Z(J+1)=A(I,I,J)                                                                000712
00534    101.          CALL  PRTPLT(A,Z,XS,YS,IP)                                                     000714
00535    102.       34 WRITE(6,33)I                                                                   000723
00541    103.       33 FORMAT(    /'     AUTO SPECTRAL DENSITY WITH RESPECT TO SERIES',I3)           000736
00542    104.          GO TO 20                                                                       000736
00543    105.          END                                                                            000741

      END OF COMPILATION:        NO  DIAGNOSTICS.
```


★ U.S. GOVERNMENT PRINTING OFFICE 1976-641-288/421 REGION NO. 4